Antarctic Science 36(2), 75–100 (2024)
doi:10.1017/S0954102023000378

Mapping of morainic complexes and reconstruction of glacier dynamics north-east of Cook Ice Cap, Kerguelen Archipelago (49°S)

PHILIP DELINE [1], HENRIETTE LINGE [2], LUDOVIC RAVANEL [1], TALIN TUESTAD [2], ROMAIN LAFITE [1], FABIEN ARNAUD [1] and JOSTEIN BAKKE [2]

[1]*EDYTEM, Université Savoie Mont Blanc, CNRS, 73000 Chambéry, France*
[2]*Department of Earth Science and Bjerknes Centre for Climate Research, University of Bergen, 5012 Bergen, Norway*
pdeli@univ-smb.fr

Abstract: Due to the limited landmasses in the Southern Hemisphere, we must rely on data from sub-Antarctic islands within the Southern Ocean to record historical climate patterns. Over the past few decades, glaciers throughout the Southern Ocean region have experienced a noticeable retreat, especially in the Kerguelen Archipelago, whose glacial landforms offer valuable insights into long-term climate fluctuations. Our comprehensive glacial geomorphological study conducted in its remote north-western region meticulously examines morainic complexes from smaller cirque glaciers and larger outlet glaciers stemming from the Cook Ice Cap. We mapped these landforms to reconstruct historical glacier extents during the Holocene. The surface area of the three main glaciers had decreased in 1962–1964 by only 35% compared to their maximum extents, whereas surface area changes across 12 time intervals spanning from 1962 to 2019 from aerial and satellite imagery reveal a cumulative reduction of 43.5%. Additionally, we modelled changes in glacier thickness and equilibrium-line altitude for the key glaciers at three distinct stages: 1) their maximum extent before 1962, 2) the early 1960s and 3) 2019. This multifaceted analysis contributes valuable insights into the dynamics of Kerguelen's glaciers and the broader implications for understanding past and ongoing climate dynamics in the Southern Hemisphere.

Received 7 September 2023, accepted 20 November 2023

Keywords: Geomorphological mapping, glacial geomorphology, moraine, sub-Antarctic zone

Introduction

The Southern Ocean is a key region for global climate dynamics and biogeochemical cycles, and its islands host valuable palaeoclimatic archives that can reveal past climate changes. One of these islands is Kerguelen, where glaciers are sensitive to the variability of the Southern Annular Mode (SAM), a large-scale atmospheric circulation pattern that affects the extratropical Southern Hemisphere. The SAM is characterized by the difference in zonal mean sea-level pressure between 40°S (mid-latitudes) and 65°S (Antarctica), and it accounts for 22% of the climatic variability in this region (Hernández *et al.* 2020). A positive SAM phase (i.e. lower atmospheric pressure on the Antarctic and higher in the mid-latitudes) tends to both strengthen and move poleward the westerlies belt, which induces reduced precipitation and increased temperature on Kerguelen (Favier *et al.* 2016, Li *et al.* 2020). Dominant in the last two decades, it caused a significant retreat of local glaciers. Therefore, the state of the SAM influences the glacial dynamics on Kerguelen, and the reconstruction of glacial history can provide insights into the long-term climate variability in the Southern Ocean.

One of the methods to reconstruct glacial history is to use moraine chronology, which is based on dating the age of moraines using techniques such as surface exposure dating. Moraines are ridges of rock debris deposited by glaciers at their margins, and they record the timing and magnitude of glacial advances in response to climate changes. Before applying surface exposure dating, it is necessary to map the moraine chronology and establish a sampling strategy.

Because the influence of the surrounding ocean buffers air temperature changes, precipitation changes are the main drivers of high-frequency environmental changes in sub-Antarctic islands. A comparison with other sub-Antarctic islands can help us to assess the regional and global significance of the glacial fluctuations on Kerguelen. South Georgia, for instance, has a rich record of palaeoclimatic archives, such as glaciers, lakes and peat bogs (Van der Putten *et al.* 2004, van der Bilt *et al.* 2017, Oppedal *et al.* 2018, Bakke *et al.* 2021). The composite reconstructions from South Georgia cover the past 14.5 ka. The deglaciation following the Antarctic Cold Reversal started *c.* 13.2 ka, then was interrupted by a cooling between 11.0 and 9.0 ka that resulted in recessional moraine formation. Four glacier advances occurred during the mid-Holocene. A drift towards a

slightly cooler climate after 4.0 ka marks the onset of the Neoglacial period characterized by centennial-scale glacier fluctuations peaking at 3.4, 2.8, 1.1 and 0.7 ka and, finally, in 1910 CE. This event chronology still needs to be confirmed on Kerguelen, but it would be essential to establishing a better spatial understanding of past climate dynamics. Previous research on the Kerguelen glaciers is presented in the following section.

Glacial landforms can capture the main changes in millennial-long climate dynamics if they can be dated accurately, mainly using *in situ* cosmogenic nuclides (e.g. Balco 2020, Schaefer *et al.* 2022). However, the complex geometry of the landforms complicates the interpretation of their accompanying cosmogenic-nuclide exposure ages. Here, we present a detailed description of glacier-related landforms and formations around one of the most remote ice caps in the world: the Cook Ice Cap (CIC) on Kerguelen. The mapping and process-based understanding of the landscape is the first step towards an improved chronology of the glacial dynamics on the archipelago.

The Kerguelen Archipelago

Geographical, geological and climatic setting

Located in the Indian region of the Southern Ocean (49°30'S, 69°30'E) with an area of 7215 km^2, the Kerguelen Archipelago is part (along with Heard and Macdonald islands) of the 1.2 million km^2 oceanic Kerguelen Plateau, the largest igneous province located in the Southern Ocean (Fig. 1a; Bryan & Ernst 2007).

The archipelago is indented by countless bays, fjords and promontories (Fig. 1b). Three regions can be approximately defined on Grande Terre (Fig. 1b): 1) the Courbet Peninsula, with lowlands hosting a myriad of lakes and peat bogs to the east; 2) the Plateau Central, with low-elevated hills separated by lakes and fjords; and 3) the mountainous western half, composed of the CIC (1049 m above sea level (asl) in 1963), the Loranchet and Société de la Géographie (1081 m asl) peninsulas to the north and the Rallier du Baty Peninsula (1262 m asl) and the Gallieni Massif with Mont Ross (1850 m asl) south of the CIC. Discovered in 1772, the archipelago is part of the TAAF (French Southern and Antarctic Lands). It is uninhabited outside of the Port-aux-Français scientific base (Fig. 1b).

The bedrock of the archipelago consists predominantly of 600–900 m-thick dark traps of tholeiitic basalts gently dipping towards the south-east that formed since 40 Ma ago (Gautier *et al.* 1990). Two large magma intrusions formed the Société de la Géographie and Rallier du Baty peninsulas. Younger volcanoes such as the stratovolcano of Mont Ross formed 2.0–0.1 Ma ago with trachyte lava flows and pyroclastic rocks (Mathieu *et al.* 2011). Plateau basalts are densely fractured, with sills and dykes of intrusive, mainly light-coloured rocks containing peridotite xenoliths (Mathieu *et al.* 2011). Precipitation of quartz geodes and carbonate minerals has resulted from hydrothermal alteration of the basalts derived from meteoric water (Renac *et al.* 2010).

The Kerguelen Archipelago is characterized by a tundra climate (0°C ≤ temperature of hottest month < +10°C) according to Peel *et al.* (2007). There are 10 weather regimes that are influenced by the SAM at seasonal and daily time scales (Pohl *et al.* 2021). Mean annual air temperature at Port-aux-Français was 4.9°C in the period 1991–2020, with 2.2°C recorded in July and 8.2°C recorded in February. Mean annual precipitation recorded at this unique permanent weather station has decreased from 815 mm in 1951–1980 to 694 mm in 1991–2020, with mean monthly minimum and maximum values of 45 mm (February) and 70 mm (May) for this last period. Since *c.* 1975, the SAM positive phase has resulted in the strengthening of SWW, both associated with an increase in precipitation, but the poleward shift has resulted in a decrease in annual precipitation at Port-aux-Français (Favier *et al.* 2016). However, due to the orographic effect of the mountains, precipitation at the station is not representative of many areas of the Kerguelen Archipelago. Mean annual precipitation at Ampère Glacier forefield, south-east of CIC, was 3155 mm from 1995 to 2001 compared to 692 mm at Port-aux-Français (Berthier *et al.* 2009).

The Global Permafrost Zonation Index Map (Gruber 2012) suggests that only warm permafrost (i.e. whose temperature is close to 0°C) is present at the highest area of Rallier du Baty Peninsula and on the west side of Mont Ross.

Characteristics of the Kerguelen glaciers and previous studies on their past extents

According to the Randolph Glacier Inventory (RGI) 6.0 (https://doi.org/10.7265/4m1f-gd79), the Kerguelen Archipelago was composed of 145 glaciers in 1963. The total glacier surface area decreased from 703 ± 51 km^2 in 1963 to 552 ± 11 km^2 in 2001 (Cogley *et al.* 2014). The CIC covered 501 km^2 in 1963, 410 km^2 in 2001 (Berthier *et al.* 2009) and 403 km^2 in 2003 (Cogley *et al.* 2014). Among the 21 CIC outlet glaciers, the second largest is the well-studied Ampere Glacier to the south-east of the CIC, being 61.5 km^2 in 2009 (Cogley *et al.* 2014). The ice divide and the summit of the CIC are positioned towards the east due to the strong contrast of precipitation related to the SWW and the leeward accumulation of windblown snow. The front retreat between 1963 and 2009 has been generally less for the glaciers west of the ice divide than those to the east (Verfaillie *et al.* 2021). The measured mass balance of

https://doi.org/10.1017/S0954102023000378 Published online by Cambridge University Press

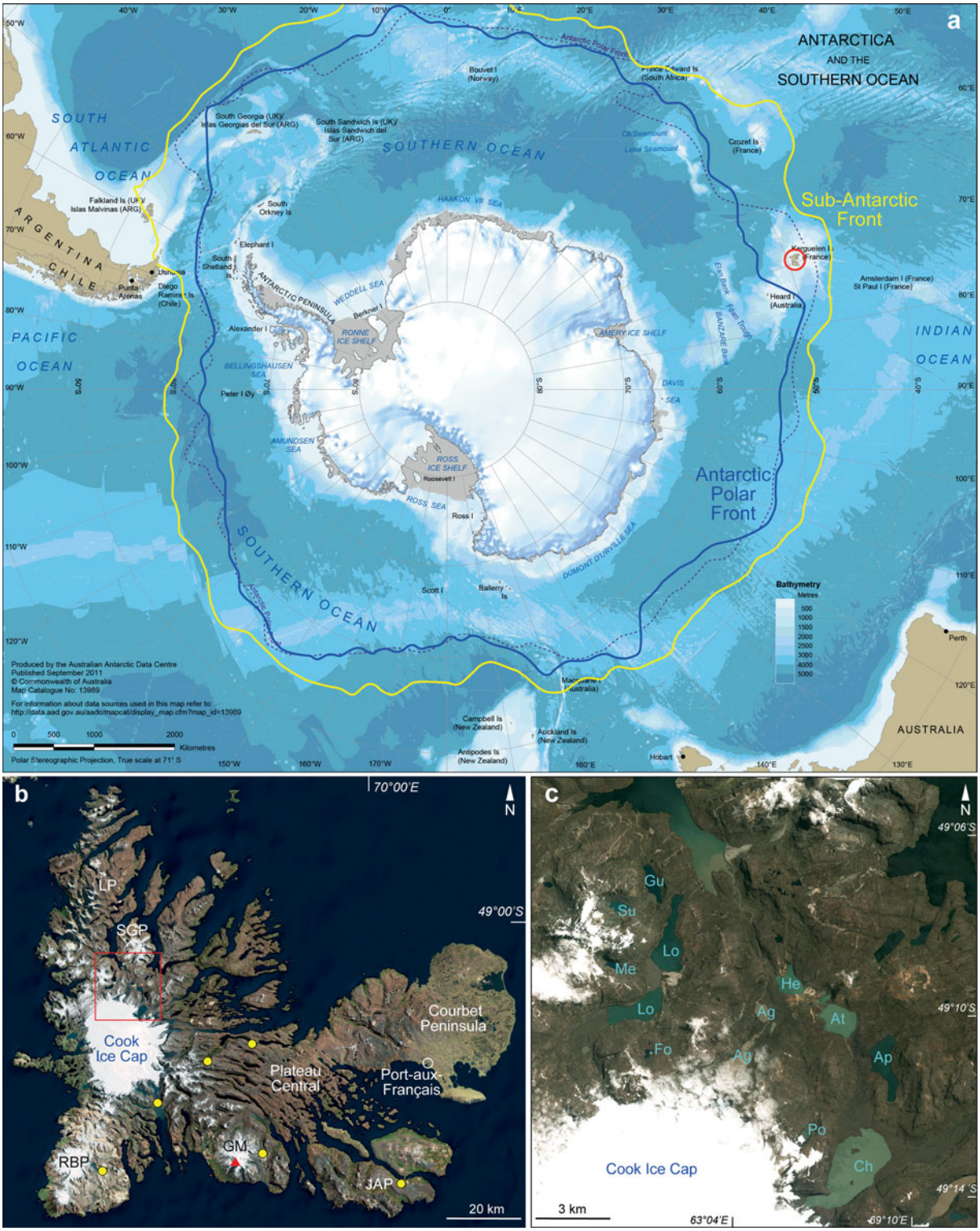

Figure 1. a. Map of Antarctica and the Southern Ocean with its hydrological fronts. Antarctic Polar Front (blue line) is located south of Kerguelen (circled in red) by Park *et al.* (2019) and Civel-Mazens *et al.* (2021), whereas Orsi *et al.* (1995) located it north of Kerguelen (dashed black line). Approximately 70% of the Antarctic Circumpolar Current is concentrated north of the Kerguelen Plateau at 45°S, whereas the other ~30% is forced through the Fawn Trough at 56°S (Park *et al.*, 2009). Map: map n° 13989 from the Australian Antarctic Data Centre. **b.** Kerguelen Archipelago. Red triangle = Mont Ross; yellow dots = previously studied moraines mentioned in the text; red square = study area (Fig. 1c). GM = Gallieni Massif; JAP = Jeanne d'Arc Peninsula; LP = Loranchet Peninsula; RBP = Rallier du Baty Peninsula; SGP = Société de la Géographie Peninsula. Satellite image: Landsat 7, November 2001. **c.** Study area. Lakes: Guynemer (Gu), Surprise (Su), Mermoz (Me), Louise (Lo; $n = 2$), Forel (Fo), Héra (He), Athena (At), Aphrodite (Ap), Agassiz (Ag; $n = 2$), Pointu (Po), Chamonix (Ch). Pléiades orthoimage from January 2019.

https://doi.org/10.1017/S0954102023000378 Published online by Cambridge University Press

the CIC decreased from -1.33 ± 0.90 to -1.59 ± 0.19 m water-equivalent per year from 1963–2000 to 2000–2010 (Favier *et al.* 2016), and its equilibrium-line altitude (ELA) has risen from 549 m asl in 1958–1963 to 677–745 m in 2000–2009 (Verfaillie *et al.* 2015). The mean elevation change rate at CIC was -1.4–1.7 m year^{-1} between 1963 and 2000 (Berthier *et al.* 2009) and approximately -1.5 m year^{-1} between 2000 and 2019 (Hugonnet *et al.* 2021).

Outside of the CIC, glaciers are present in three main areas (Fig. 1b): the Rallier du Baty Peninsula, the Gallieni Massif and, more marginally, the Société de la Géographie Peninsula, with a total surface area of 119 km^2 in 2001 compared to 179 km^2 in 1964 (Cogley *et al.* 2014). Finally, the small Guynemer and Mermoz glaciers are located north of the CIC near Pic Guynemer (1097 m; Fig. 2).

Research on the past Kerguelen glaciers began with Aubert de la Rüe (1932) but has mainly been developed since the start of the twenty-first century. Based on the distribution of the scoured bedrock surfaces, till deposits and erratic boulders, Aubert de la Rüe (1932, 1967) concluded that the whole archipelago was covered by ice in the past. However, glacial refugia during the Last Glacial Maximum (LGM) are suggested by present-day plant species at the bottom of organic peat accumulations during the Late Glacial in the Courbet Peninsula (Van der Putten *et al.* 2015). Other studies (e.g. Nougier 1970) suggested that fjords and U-shaped valleys formed well before a restricted LGM ice cover. Conversely, Hall (1984) suggested that they resulted from a more extensive LGM ice cover with an ELA at ~200 m asl, while Jomelli *et al.* (2017, 2018) dated erratic boulders and bedrock from Marine Isotope Stage (MIS) 2 and MIS 3 ages on the Plateau Central and Courbet Peninsula (Fig. 1b).

Moraines have been used to reconstruct past extents for several glaciers on the Kerguelen Archipelago (see locations in Fig. 1b). Nonetheless, no detailed maps of a morainic complexes (here defined as a set of recessional moraines deposited upstream of a terminal one that mark stages of glacier advances or stillstands) have been produced, except that for Gentil Glacier (Charton *et al.* 2020). At Ampere Glacier, the most studied glacier on the Kerguelen Archipelago (Vallon 1977a,b, Frenot *et al.* 1993, 1997, 1998, Jomelli *et al.* 2017, Verfaillie *et al.* 2021, Charton *et al.* 2022), a terminal moraine and four sets of recessional moraines of Late Holocene age were deposited between 1150 and 250 m away from the 1962 front. Downstream, a 1.3 km-long right-lateral moraine damming Lake Jaune is the only moraine visible on satellite images in the 2.5 km-wide outwash plain, which should correspond to a glacier front located at least 2.5 km away from that of the 1962 front. Finally, a 1 km-long and 4 m-high submarine frontal moraine is suggested by multibeam bathymetry of the fjord Baie de la Table, which is -120 m asl and 20.5 km away from the 1962 front (Jomelli *et al.* 2017).

The Arago Glacier (Rallier du Baty Peninsula) deposited several moraines before the 1960s (Charton *et al.* 2022). A first set of at least seven Late Holocene frontal moraines dams Lake Arago. The outermost moraine is at a maximum distance of ~500 m from the 1962 front. At 7 km down-glacier, a frontal moraine of Late Glacial age has been deposited in a narrow valley by a diffluent lobe (Charton *et al.* 2022). No other moraines have been surveyed in the ~2 km-wide Larmor outwash plain.

The Gentil Glacier (Gallieni Massif) flows from the steep and high east slope of Mont Ross, from where frequent rockfalls detach. The glacier is therefore heavily covered with debris, just like the nearby Buffon Glacier. The innermost moraine of Late Holocene age is ~250 m away from the present glacier front, and a terminal moraine was deposited ~1.5 km away from the innermost one, with a series of recessional moraines in between, both of Late Glacial age (Charton *et al.* 2020).

Located between the CIC and Plateau Central, the Late Glacial Bontemps moraine (Jomelli *et al.* 2017, 2018) was deposited 25 km down-glacier of the 2021 front of the Vallot Glacier, with a small set of recessional moraines present ~350 m upstream. At 15 km upstream, an outermost set of frontal moraines was deposited in Val Travers by the then-merged Explorateur and Ampère glaciers, with a second set ~1.5 km upstream, 12 km away from the present Explorateur front; both are of Late Glacial age (Charton *et al.* 2022).

Finally, in the Jeanne d'Arc Peninsula, two ~600 m-long Late Glacial moraines were deposited by a former cirque glacier on the north slope of the Belvedere Plateau (Jomelli *et al.* 2018).

No glacial geomorphological study has been carried out in the Guynemer-Chamonix region until our investigation.

Study area: the Guynemer-Chamonix region, north-east of the Cook Ice Cap

The study region is characterized by two main areas (Fig. 2):

1) The CIC basin comprises three outlet glaciers, Forel, Agassiz and Chamonix glaciers; the smaller Pointu Glacier is no longer connected to the CIC, whereas Table and Lune glaciers are reduced to patchy ice. Several lakes are fed by glacial meltwater, but not Lake Aphrodite anymore (Fig. 2). The rivers flow through a deep gorge or a steep rock step before they reach the fjord Baie du Repos. The basalt plateaus

https://doi.org/10.1017/S0954102023000378 Published online by Cambridge University Press

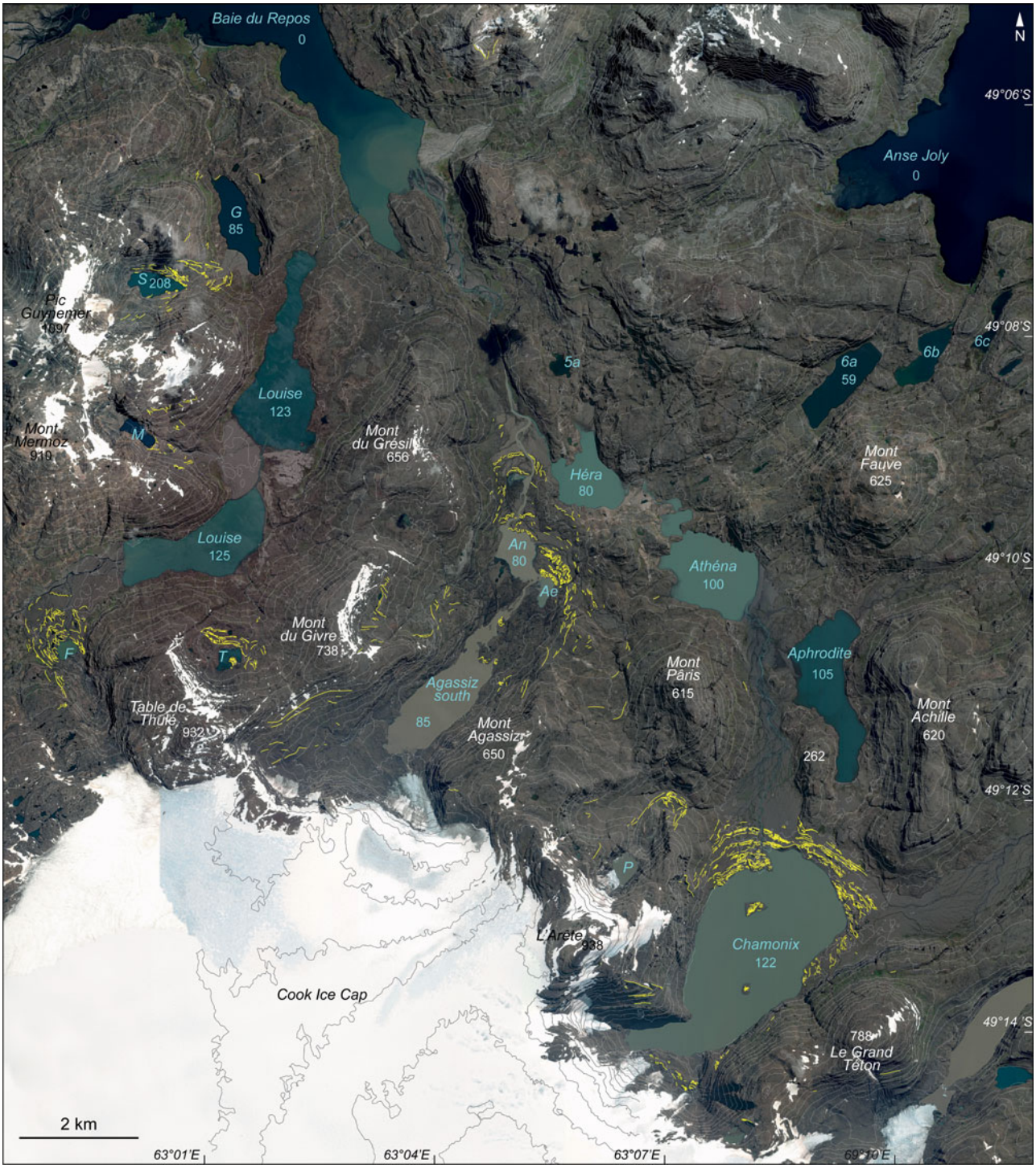

Figure 2. Study area north-east of Cook Ice Cap. Moraine crest lines in yellow. The colour of the lakes and fjords, a proxy of their turbidity, varies according to their connection to glacial meltwater. Pléiades orthoimage from 2021 (Bing Aerial); contour interval: 25 m; elevation: metres above sea level.

culminate at 500–700 m asl, to peak at 900 m along the north-east margin of the CIC.

2) The Guynemer Massif is a basaltic stratovolcano that peaks at Pic Guynemer (1097 m asl), on which the small Guynemer and Mermoz glaciers remain.

Lake Guynemer is the larger (0.64 km^2) in the massif, and lakes Surprise and Mermoz did not exist in 1964. Glacier-fed lakes range from 0.11 km^2 (Mermoz) to 5.68 km^2 (Chamonix) and covered a total area of 16.78 km^2 in 2021. More than 3000 other lakes are

https://doi.org/10.1017/S0954102023000378 Published online by Cambridge University Press

present in the study area, most being very small and formed in the last decades following the shrinkage of the glaciers (Fig. 2).

The Guynemer-Chamonix region exhibits a characteristic glacial landscape. Scoured bedrock surfaces, till deposits, moraines and erratic boulders serve as evidence of the palaeoglaciation of the region, but periglacial processes dominate the present morphodynamics (Fig. 2). Regolith landforms resulting from frost weathering and heaving cover flat terrain and slopes; basaltic bedrock outcrops only as roches moutonnées and fluvial bedrock gorges, or rather as sub-vertical rock scarps. Due to freeze-thaw cycles, talus sheets and cones accumulate at the foot of these scarps, some of which are reworked by debris flows, supra-nival sliding of debris and snow avalanches. Blockfields are on gentle slopes and flat areas, with patterned ground resulting from frost heaving due to ice segregation. Frost shattering produces the comminution of the boulders. Permafrost may be present in three high-elevated sites according to the fringe of the uncertainty of the Global Permafrost Zonation Index Map (Gruber 2012): the top of Guynemer Massif, Table de Thulé and the Arête above Pointu Glacier.

Fractures and dykes that cut the rock scarps concentrate the drainage into waterfalls. Braided rivers drain the depression downstream of Lake Guynemer and the wide valleys downstream of Lake Chamonix. Other river sections are meandering (e.g. in the confluence area of Agassiz and Hera rivers) or flow through a rock gorge (e.g. downstream Lake Surprise). Active sediment deposition built large fan-deltas at Lake Guynemer and Lake Louise and infilled the valleys downstream of Lake Chamonix (Fig. 2).

Finally, vegetation is generally restricted to scarce moss patches in rills and other wet sites, with few Kerguelen cabbages (*Pringlea antiscorbutica*), endemic to several islands of the Southern Ocean. Below 250 m asl, the vegetation cover is more continuous on inactive rockfall talus sheets and peat bogs.

Data sources and methods

Glacial geomorphological mapping

A multi-method mapping approach was utilized in the study (Chandler *et al.* 2018). To enable the detailed geomorphological mapping of glacial landforms, a high-resolution digital elevation model (DEM) and an orthoimage with spatial resolutions of 2.0 m and 0.5 m, respectively, were produced from a tristereo set of Pléiades 1A images, acquired for this study on 16 January 2019 (Table I). The processing has been performed using *PC Geomatica* software, with a normalized cross-correlation method used for extracting the DEM and using ground control points extracted from Google Earth imagery. To remove artefacts related to the DEM processing, the data were filtered using a multi-directional Lee filter procedure in *SAGA GIS* (Ruiz & Bodin 2015).

Before fieldwork, several moraines were recognized and remotely mapped in the study area thanks to the high resolution of these data. Detailed mapping was carried out in the field in November and December 2019 in the Guynemer basin and in the glacier forefields of Agassiz, Pointu and Chamonix glaciers, downstream of their respective lakes. In the field, we also obtained high-resolution images of these areas from DJI Phantom III drone flights and took ground photographs, which improved the mapping detail and accuracy. Other sites of the study area have subsequently been mapped in detail from remote sensing, using 2019 and 2015 Pléiades-derived DEMs and orthoimages, a 2017 Google Earth orthoimage and a 2021 Bing Satellite orthoimage to palliate persistent cloud and snow covers or shadows in some areas, with few image deformations.

Moraines and moraine crests have been comprehensively mapped in the study area. Other glacial landforms such as roches moutonnées, hummocky moraines, moraine breaches, gullied moraine walls, bouldery sheets, meltwater channels and sandurs have been locally mapped, as some non-glacial landforms (e.g. rockfall deposits, active and inactive outwash surfaces, beaches, gullies, gorge rims) do not appear on our maps. By contrast, an exhaustive mapping of the lakes has been carried out, as many of these lakes formed following the shrinkage of glaciers, as has been observed worldwide (Shugar *et al.* 2020).

Reconstruction of glacier extents prior to the 1960s

The 2D reconstruction of three glacier extents is based on the morphological markers related to the palaeoglaciers, mainly the moraines. The 3D surface of our reconstructed maximum extents of Guynemer and Chamonix glaciers was obtained by 1) drawing contour lines in *QGIS* with an interval of 50 m, then 2) interpolating in *GlaRe* to produce a DEM. Agassiz Glacier surface and thickness reconstruction was performed with the *ArcGIS* toolbox *GlaRe*, although it is not well suited to ice-cap outlets (Pellitero *et al.* 2016). Using a numerical approach, *GlaRe* computes ice thickness along manually drawn palaeoglacier flowlines by iteratively solving an equation that assumes no basal sliding and perfect plasticity for ice rheology (Pellitero *et al.* 2016). Basal shear stress is manually tuned along the flowlines, from 100 kPa on the steep, rough terrain, in the cirque and below the CIC to 50 kPa in the flat and soft-sediment areas where the tongue of the

https://doi.org/10.1017/S0954102023000378 Published online by Cambridge University Press

Table I. Set of aerial and satellite images used in this study. Metadata of IGN-TAAF surveys from 1969, 1971 and 1974 that we used were not retrieved, but instrument stripes and the four fiducial marks on the aerial photographs are similar from 1962 to 1971.

Year/ month	Area of interest	System	Reference number	Scale or resolution	Bands	Acquisition	Source
1962–1963	Forel	HB SOM view camera[a]	C93PHQ2681_1962_TAAF_KER_XLVII_0215	1:20 240	B&W		Remonter le temps IGN
1962–1963	Table	HB SOM view camera[a]	C93PHQ2681_1962_TAAF_KER_XLVII_0212	1:20 240	B&W		Remonter le temps IGN
1962–1963	Agassiz	HB SOM view camera[a]	C93PHQ2681_1962_TAAF_KER_XLVII_0207	1:20 240	B&W		Remonter le temps IGN
1962–1963	Pointu	HB SOM view camera[a]	C93PHQ2681_1962_TAAF_KER_XLVII_0202	1:20 240	B&W		Remonter le temps IGN
1962–1963	Chamonix	HB SOM view camera[a]	C93PHQ2681_1962_TAAF_KER_XLVII_0200	1:20 240	B&W		Remonter le temps IGN
1963–1964	Guynemer	HB SOM view camera[a]	C93PHQ2191_1964_TAAFKERXVI_0007	1:23 202	B&W		Remonter le temps IGN
1963–1964	Mermoz	HB SOM view camera[a]	C93PHQ2191_1964_TAAFKERXVI_0006	1:23 202	B&W		Remonter le temps IGN
1964–1965	Agassiz	HB SOM view camera[a]	C93PHQ2341_1965_TAAF_KER_XXXI_0316	1:28 800	B&W		Remonter le temps IGN
1964–1965	Chamonix	HB SOM view camera[a]	C93PHQ2341_1965_TAAF_KER_XXXI_0322	1:27 200	B&W		Remonter le temps IGN
1969–1970	Agassiz	HB SOM view camera[a]	C93PHQ2631_1969_TAAFKERI_0067	1:17 600	B&W		Remonter le temps IGN
1969–1970	Pointu	HB SOM view camera[a]	C93PHQ2631_1969_TAAFKERI_0058	1:17 600	B&W		Remonter le temps IGN
1969–1970	Chamonix	HB SOM view camera[a]	C93PHQ2631_1969_TAAFKERI_0053	1:17 600	B&W		Remonter le temps IGN
1971	Agassiz	HB SOM view camera[a]	C93PHQ2731_1971_TAAFKER_0068	1:8000	B&W		Remonter le temps IGN
1971	Pointu	HB SOM view camera[a]	C93PHQ2731_1971_TAAFKER_0062	1:8000	B&W		Remonter le temps IGN
1971	Chamonix	HB SOM view camera[a]	C93PHQ2731_1971_TAAFKER_0058	1:8000	B&W		Remonter le temps IGN
1974	Chamonix	HB SOM view camera[a]	C93PHQ2961_1974_TAAFGLACIERCOOK_0047/50	1:23 335	B&W		Remonter le temps IGN
1991/09	Whole study area	SPOT 2 HRV 2	2 232-449 91-09-08 05:07:08 2 P	10 m	PAN	Mono	Spot World Heritage CNES
1994/03	Forel to Chamonix	SPOT 3 HRV 1	3 232-450 94-03-03 05:22:06 1 P	10 m	PAN	Mono	Spot World Heritage CNES
2001/11	Whole study area	Landsat 7 ETM+	LE71390942001331SGS00	30 m	MS	Mono	EarthExplorer USGS
2007/02	Agassiz	SPOT 5 HRS 2	5 233-450 07-02-15 05:07:41 2 S	2.5 m	MS	Mono	Spot World Heritage CNES
2009/12	Whole study area	SPOT 5 HRS 2	5 233-450 09-12-21 05:07:12 2 S	2.5 m	MS	Mono	Spot World Heritage CNES
2015/02	Forel to Chamonix	Pléiades 1B	DS_PHR1B_201502220516506_FR1_PX_E069S50_0220_00823	0.5 m[b]	MS	Stereo	Spot World Heritage CNES
2017/03	Whole study area	Pléiades 1A	DS_PHR1A_201703160524025_FR1_PX_E069S50_?	0.5 m[b]	MS	Tristereo	Google Earth via WMS
2019/01	Whole study area	Pléiades 1A	DS_PHR1A_201901160513269_FR1_PX_E069S50_0121_01703/696/690	0.5 m[b]	MS	Tristereo	ISIS programme CNES
2021	Whole study area	Pléiades	?	0.5 m[b]	MS	?	Bing Aerial via WMS

B&W = black and white; MS = multispectral; PAN = panchromatic; WMS = Web Map Service.
[a]HB: Helicopter-borne film camera (18 × 18 cm SOM view camera).
[b]Pan-sharpened image.

maximum Agassiz Glacier extended (Cuffey & Paterson 2010, Pellitero *et al.* 2016).

The use of *GlaRe* requires a complete DEM of the glacier bed topography, which necessitates the removal of present lakes and glaciers from our DEM. A bathymetric survey was carried out at Lake Guynemer in 2014. We propose a realistic bathymetry for lakes Surprise, Agassiz and Chamonix through the digitalization of possible 10 m contour lines in *QGIS*, guided by the surrounding topography (including bedrock structures) and the presence of islands. This was then imported and interpolated by triangulation into *SAGA GIS* to be finally integrated into the DEM. At Lake Guynemer, the volumes of a large post-glacial fan-delta and a 20 m-thick lacustrine sediment deposit (a conservative thickness based on a 2014 coring) have been removed from the DEM in the same way. Outwash deposits downstream of lakes Agassiz south and Chamonix have not been removed, as no data are available regarding their thickness.

No geophysical data exist for the thickness of the CIC, and modelling by Millan *et al.* (2022) based on 1962 data is too large-scale. To determine the CIC glacier bed topography, we first implement a CIC surface DEM derived from 2015 Pléiades images in our DEM, as cloud cover on 2019 images masked most of the CIC surface. Then the 2015 CIC thickness was removed using *GlabTop*, although this tool has been designed for valley glaciers rather than ice caps, which increases the uncertainty in the results (Linsbauer *et al.* 2012, Paul & Linsbauer 2012). Besides the surface DEM, *GlabTop* requires glacier outlines to calculate ice thickness from the surface slope, assuming a relation between the basal shear stress and the glacier elevation range as a governing factor of mass turnover. It requires the manual digitization of branch lines from the bottom to the top of the glacier perpendicular to the contour lines of surface elevation, with one parallel line for every 200–400 m of glacier width, ending ~100 m before the glacier outline, along which ice thickness is estimated (Magnin *et al.* 2020).

Reconstruction of glacier extents since the 1960s

During a 1961–1962 summer campaign in Kerguelen, 1900 oblique aerial photographs (13 × 18 cm and 6 × 6 cm; black and white and colour) were taken from a helicopter in order to map most of the glaciers of the archipelago (Bauer 1963). The four reconnaissance sketches produced at the scale of ~1:100 000 represent a total of 78 glaciers, including those in our study area (Fig. S1). The first vertical aerial images in the Guynemer-Chamonix region (and in the archipelago) were taken from a helicopter by TAAF operators with a view camera (18 × 18 cm, SOM brand) in 1962–1963, followed by similar surveys in 1963–1964, 1964–1965 and 1965–1966 that focused on different glaciers of the study area (Table I). The topographic map of the Kerguelen Archipelago at the scale of 1:100 000 released in 1967 by the French mapping agency IGN was based on these images (Durand de Corbiac 1970).

The first satellite image available for our study area is a SPOT 1 image from 4 March 1986, but this was unusable due to clouds obstructing the view of the glacier fronts and extents in the Guynemer Massif and other glaciers of the study area being outside the image. The first usable satellite image is a SPOT 2 image from September 1991. The first Landsat image for our study area is from November 1999 but is largely cloudy; Landsat images until 2012 have only a 30 m resolution (Table I). Several SPOT images with 10 m then 2.5 m resolutions were used up to 2009, while 0.5 m resolution Pléiades images have been available since 2015 (Table I).

Since the covering between TAAF aerial images is limited to a unique stripe of images with strong deformation on their edges, we georeferenced each selected image (Table I) in the GIS by adjusting it to the orthoimages from the 2015, 2017 or 2019 Pléiades images through the selection of ~30 ground control points for each image. While SPOT images are correctly georeferenced for lowlands in our study area, they needed to be adjusted to each elevated site. As a result, uncertainty in the mapping varies according to the aerial and satellite images. For instance, the extent of Guynemer Glacier on the south side of the Lake Surprise basin in 1962 has to be considered cautiously due to the steep slope, as a small offset in the plane generates change in elevation.

While aerial photographs and satellite images of Agassiz, Pointu and Chamonix glaciers are available for many years in the period 1962–2021, other glacier basins of the study area are less well documented after 1962 due to the absence of TAAF flight surveys or due to clouds on satellite images. For instance, only Chamonix Glacier is present in the 1974 images (Table I). When abundant snowpack made glacier delineation difficult for a particular year, we used images from the nearest year or adapted glacier limits according to local topography. Large snowfields could be confused with glacier extent in the upper margins of Forel, Table or Agassiz glaciers, in the Guynemer basin in 1962–1965 and in the north-west area of Pointu Glacier between 1994 and 2009. Delineations from 2019 images were similarly checked/modified from 2017 images where snow or clouds were present. The ice divide of CIC was delineated with a DEM from the 2015 Pléiades images and considered representative for 1963 and 2021; it slightly differs from that of Verfaillie (2014, fig. 1.2) based on other data.

The 3D glacier surface of 1962–1963 was reconstructed with *GlaRe* for Guynemer and from the digitalization of

https://doi.org/10.1017/S0954102023000378 Published online by Cambridge University Press

the contour lines of the IGN map for Agassiz and Chamonix glaciers. The present 3D glacier surfaces come from the DEMs from 2019 for Guynemer Glacier and from 2015 for the two other glaciers.

Computation of ELA in the study area

Once the 3D surface of a glacier has been reconstructed, ELA can be estimated. The ELA is the elevation at which net gain and net loss are equal, and it can be used 1) to track how the glacier mass balance changes over time in response to local past climate forcing and 2) to compare the mass balance of local glaciers with different extents and shapes at a given time. Various methods are proposed to estimate the ELA (Benn & Lehmkuhl 2000). As the debris transported by a glacier from its accumulation zone is deposited on the margins of its ablation zone, we used the maximum elevation of lateral moraines (MELM; Torsnes *et al.* 1993) to approximately estimate the ELA of several glaciers in the early 1960s. Several computational methods exist to estimate the ELA, from an *Excel* spreadsheet (Benn & Gemmell 1997) to an approach based on continuity equations (Keeler *et al.* 2021). For ELA estimates before the 1960s, we considered the widely applied accumulation area ratio (AAR) using the *ArcGIS* toolbox by Pellitero *et al.* (2015). The AAR technique postulates that the ratio between accumulation and ablation areas is constant for a steady-state glacier. The typical AAR value for a steady-state ELA is 0.6, although it actually varies between 0.4 and 0.8 (Dyurgerov *et al.* 2009) and it does not consider the mass balance gradient, which is steeper on maritime glaciers, nor the area-altitude distribution of the glacier surface (Pellitero *et al.* 2015). However, we used this value of 0.6 as an average AAR of 0.58 has been proposed for a set of outlet glaciers mainly located in Norway and Iceland with climatic conditions similar to those of Kerguelen (Ignéczi & Nagy 2013). This value is valid for steady-state glaciers that are depositing well-developed moraine sequences, such as several sets of the morainic complexes of Guynemer, Agassiz and Chamonix glaciers; by contrast, these glaciers were probably in a period of recession at the onset of the 1960s, and surely so at the end of the 2010s. Finally, the AAR method underestimates the ELA change for a glacier flowing onto a flat area because glacier hypsometry is not considered (Torsnes *et al.* 1993), whereas water-terminating glacier ELA is probably unrepresentative of climatic conditions (King *et al.* 2018, Carrivick *et al.* 2022).

Results

Guynemer Glacier foreland and morainic complex

The deep U-shaped upper basin of the Guynemer area is occupied by Lake Surprise (0.25 km^2) and the Guynemer Glacier, which had shrunk to 0.7 km^2 in 2019 with a regenerated front at 340 m asl. Downglacier, Lake Guynemer (0.65 km^2), whose maximum depth is 90 m, is located in another deep U-shaped basin; its outlet river has incised a narrow gorge through the scoured Goéland hill towards the north, whereas a wide fan-delta at the south-west end of the lake was formed by sediment supply from the upper Guynemer basin. Forty-five smaller lakes are also present throughout the basins (Fig. 3).

Around the glacier overdeepening that hosts Lake Surprise, Mg-7 moraines are the youngest of the Guynemer morainic complex, reflecting a dozen glacier front positions since the 1960s. These latero-frontal moraines with matrix-supported till are of a metric size, except for a 30 m-high left lateral moraine on the north shore built by superposition as suggested by its size (Fig. S2a). Mg-6 is mainly formed by a left latero-frontal moraine generally with till that predates the 1962 extent; downstream, two main latero-frontal moraines with clast-supported till constitute Mg-5 and Mg-4, which continue on the south side for over 300 m. The corresponding glacier fronts were located ~230, 360 and 550 m downglacier of the 1962 extent, respectively; rounded boulders of pluridecimetric size dominate in the upper sections of the three sets (Fig. 4a). Mg-3 is the outermost moraine in the upper basin; angular to sub-angular large boulders suggest that rockfalls from the close rock cliffs supplied debris to the left margin of the glacier at that time (Fig. 4b).

Very few moraines are present around Lake Guynemer. Mg-2 is composed of two short lateral moraines of a metric size with matrix-supported till with large rounded boulders, interrupted by a 30 m-high rock cliff (Fig. 4c) and a ~5 m-high frontal moraine on the north shore of Lake Guynemer with a dozen sub-angular boulders of a metric size on its surface (Fig. 4d); when the glacier occupied the overdeepening, its front was ~2.2 km away from that of 1962. Finally, Mg-1 is a moraine of a metric size with matrix-supported till, with a ~5.5 m-high boulder deposited ~100 m above and east of the lake (Fig. S2c). A few short moraines are deposited between 110 and 150 m asl at the left bank of the outlet.

Agassiz Glacier foreland and morainic complex

The Agassiz Glacier (~17 km^2) flows from the CIC dome down to 205 m asl. Its basin is a ~7 km-long valley, whose deep U-shaped upstream area is now occupied by Lake Agassiz south (1.5 km^2), located between Mont du Givre (738 m asl) and Mont Agassiz (650 m; Fig. 5). Two wide cirques are carved on the west side of the valley, whereas the east side opens towards Lake Athena.

https://doi.org/10.1017/S0954102023000378 Published online by Cambridge University Press

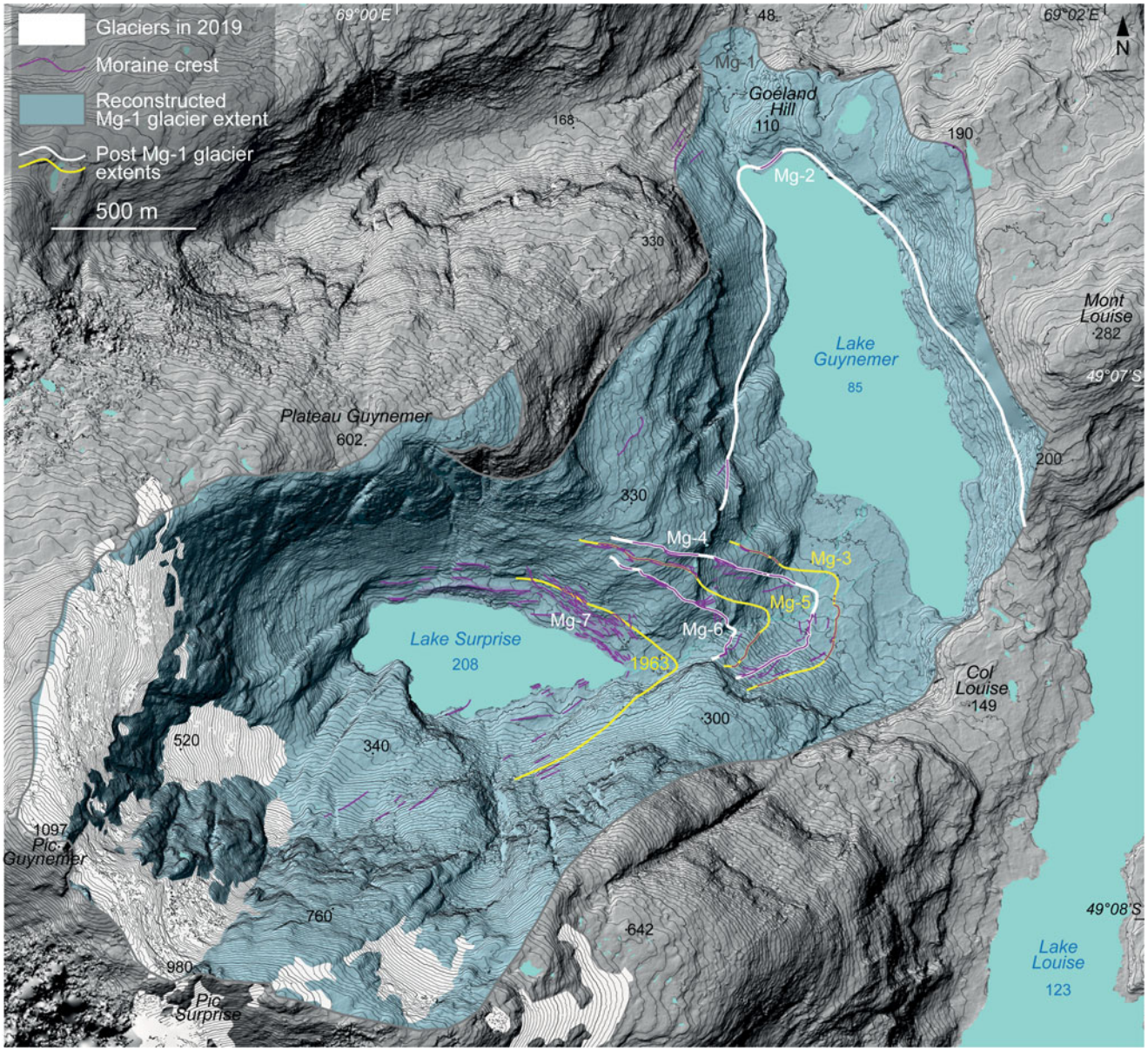

Figure 3. Guynemer Glacier morainic complex, with Mg-1 to Mg-7 moraine sets and the 1963 front position (the alternation of white and yellow colours allows them to be better distinguished). Topographic map from Pléiades-derived digital elevation model; contour interval: 5 m; elevation point in metres above sea level.

Two other wide lakes and > 700 much smaller lakes are present in the basin.

The glacier forefield is divided by a ~20–60 m-high rock cliff that towers over Lake Agassiz east (Fig. 5). The main frontal moraine sets and several lateral ones are deposited to the north of the rock cliff (Figs 6 & S3). Lateral moraines are mostly exclusive to the upstream area and are found mainly on the right side of the basin.

Few moraines have been deposited since 1965. Ma-9 and Ma-10 are 1) two groups of small frontal moraines on the shore of Lake Agassiz south, deposited ~750 m and 1.4 km upstream from the 1965 glacier front position, and 2) some of the left-lateral moraines at the head of the basin at >200 m asl. Ma-9 and Ma-10 were probably deposited shortly before 1991 and 2001, respectively (see below). Possible frontal moraines corresponding to the glacier extent of 1962–1965 have probably been eroded or buried by the outwash sediments.

Ma-8 moraines dam Lake Agassiz east. Ma-7 is a set of mainly frontal moraines with matrix-supported till, ~400 m long and up to ~5 m high, located ~350–400 m downglacier of the 1965 glacier front (Fig. S4a,b). Ma-8 and Ma-7 are separated by a ~40 m-wide meltwater channel connected to the east side of the lake. Merging

https://doi.org/10.1017/S0954102023000378 Published online by Cambridge University Press

Figure 4. a. Latero-frontal moraines with clast-supported till and rounded boulders above the north shore of Lake Surprise (from Mg-4 in the foreground to Mg-5 and Mg-6); the difference in altitude is ~50 m. **b.** Latero-frontal moraines with clast-supported till and angular boulders supplied by rockfalls (foreground: Mg-3; background: Mg-4); crest elevation of Mg-3 is 110 m above sea level (m asl). **c.** A 3 m-high lateral moraine Mg-2 (185 m asl), ~100 m above Lake Guynemer. **d.** A 5 m-high frontal moraine with matrix-supported till Mg-2 (90 m asl) on the north shore of Lake Guynemer.

with Ma-7 at the south end, Ma-6 is the best-preserved set of moraines of the Agassiz complex. Ma-6 moraines with matrix-supported till are mainly composed of 1) a ~1 km-long sinuous latero-frontal moraine, up to ~15 m high, cut by a ~30–50 m-wide, curved meltwater channel (Fig. S4a), and 2) right-lateral moraines with large rounded boulders above the rock cliff, up to ~10 m high (Fig. S4c). At the head of the basin, traces of two long left-lateral moraines standing 30–80 m above the 1965 glacier surface could correspond to the frontal ones of Ma-8, Ma-7 and/or Ma-6.

The downstream part of Ma-5 comprises a set of ~10 m-high frontal moraines with matrix-supported till that dam Lake Agassiz north, 750 m away from two small lateral moraines with clast-supported till at the foot of the rock cliff (Fig. 7a). Upstream from the rock cliff, Ma-5 can be followed over ~1.3 km up to 250 m asl, generally in a trace state. Ma-4 is best preserved upstream of the rock cliff at ~125–150 m asl, with small moraines formed by clast-supported till on the edge of bouldery sheets (Fig. 7b); in the distal part of Ma-4, some eroded moraines protrude from the sandur beyond Ma-5. By contrast, the 60–100 m-wide Ma-3 frontal group is distributed across the entire width of the valley floor (Fig. 8a), with ~5 m-high moraines with matrix-supported till mainly composed of rounded gravels and boulders of a decimetric size (Fig. S5a,b); moraines on the valley side are rare. The Ma-3 glacier front was at ~1.1 km away from that of 1965, probably with a tributary glacier flowing from Cirque de la Lune.

Ma-2 is a set of 450–650 m-long frontal moraines with matrix-supported till with abundant sub-angular boulders that constrains the river course and allows the seasonal flooding of the upstream outwash plain (Figs 8b & S5c). Ma-2 comprises sections of left-lateral moraines over ~700 m, and two short right-lateral moraines are probably deposited on the south side of Hera Pass at ~125 m asl (Fig. S6a).

The latero-frontal moraines of Ma-1 deposited on the valley floor document a > 700 m-wide glacier lobe that

https://doi.org/10.1017/S0954102023000378 Published online by Cambridge University Press

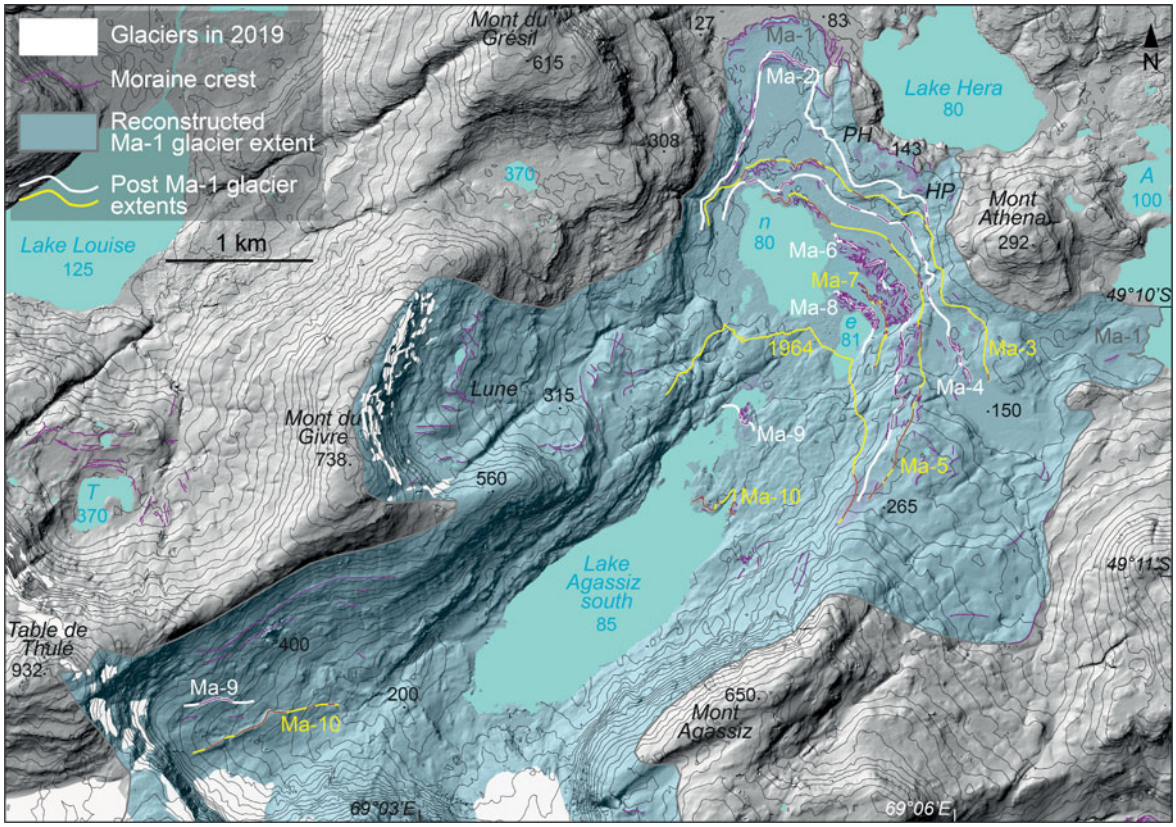

Figure 5. Agassiz Glacier morainic complex, with Ma-1 to Ma-10 moraine sets and the 1964 front position. The glacier east lobe for Ma-1 extent arbitrarily corresponds to the current shore of Lake Athena. Light purple = moraines. A = Lake Athena; HP = Hera Pass; n and e = Lake Agassiz north and east, respectively; PH = Plateau Hera; T = Lake Table. Topographic map from Pléiades-derived DEM; contour interval (low quality): 25 m; elevation point in metres above sea level. Zoomed-in image on the downstream area (Ma-1 to 1965 front) is available in Fig. S3.

Figure 6. General view of the downstream area of the Agassiz Glacier forefield. Lakes Agassiz (~80 m above sea level (m asl)) south on the left, east in the foreground and north in the background. Frontal moraines of Ma-5, Ma-3 and Ma-2 at the north shore of Lake Agassiz; latero-frontal moraines of Ma-8, Ma-7 and Ma-6 along the lakes on the right; upstream Ma-6 bouldery moraine in the foreground. In the background on the left, Pic Guynemer (1097 m asl) points between Mont du Givre (738 m) on the left and Mont du Grésil (656 m) on the right.

https://doi.org/10.1017/S0954102023000378 Published online by Cambridge University Press

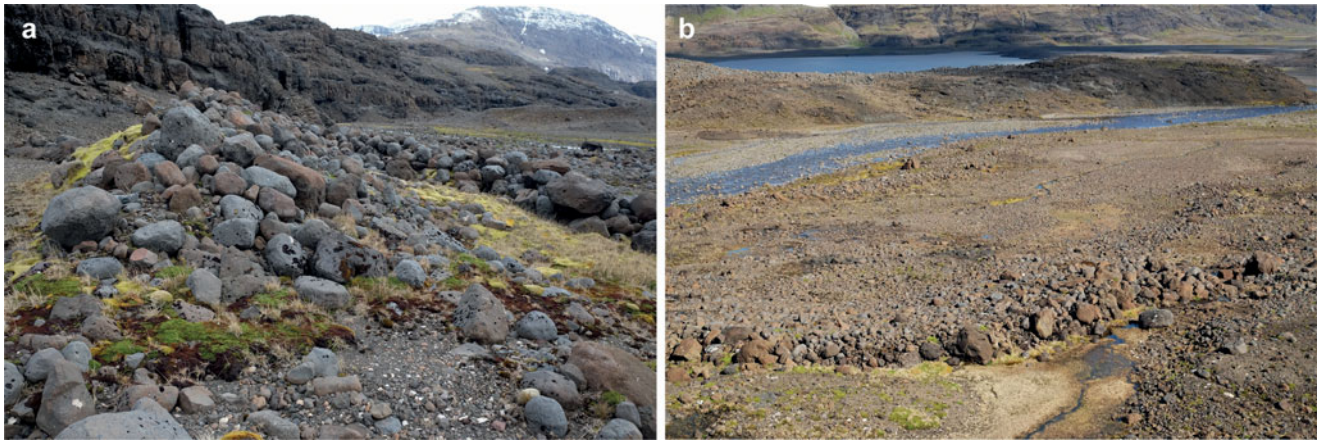

Figure 7. a. Small Ma-5 right-lateral moraines (90 m above sea level (m asl)) beneath the foot of a ~20 m-high rock cliff. **b.** A 1–2 m-high Ma-4 right-lateral moraine with matrix-supported till, on the edge of a bouldery sheet (140 m asl). On top of the rock ridge beyond the river: Ma-5 right-lateral moraines upstream of the rock cliff. In the background, Lake Agassiz north with Ma-5 frontal moraines on its right.

Figure 8. a. Southward view of 5 m-high Ma-3 frontal moraines in the foreground, Ma-5 ones along Lake Agassiz north and rare Ma-4 ones in between. **b.** Southward view of 10 m-high Ma-2 frontal moraines in the foreground and Ma-1 ones 250 m beyond with the lateral moraine on the right of the river. **c.** Southward view of a right-lateral moraine with matrix-supported till Ma-1 (Lake Hera in the background on the left).

https://doi.org/10.1017/S0954102023000378 Published online by Cambridge University Press

was ~2.1 km downglacier from that of 1964 (Fig. 8b,c). Right-lateral moraines and boulder sheets with rounded debris onto Plateau Hera suggest that the glacier overflowed towards Lake Hera (Fig. S6b).

Chamonix Glacier foreland and morainic complex

The Chamonix basin is mainly occupied by a ~4.5 km-long lake and a CIC outlet glacier (~12 km^2) that flowed down to ~200 m asl in 2021. Lake Chamonix (5.7 km^2) has steep sides between Arête, Hublots and Grand Téton (Fig. 9). Then the basin opens up to the east into a wide valley and to the north into a U-shaped valley between Mont Pâris and Mont Achille, divided by the scoured Mont Aphrodite in a west arm with an outwash plain up to 1.2 km wide and an eastern one mainly occupied by Lake Aphrodite (1.7 km^2). The small Cirque West is carved on the east flank of the Croupe.

The Chamonix morainic complex is mainly formed by at least eight sets of latero-frontal moraines that surround the northern half of the lake (Figs 9 & S7). The outermost Mc-1 has largely been eroded or buried; moraines with clast-supported till and bouldery sheets with rounded boulders are preserved on the gentle slope at the foot of the south side of Mont Aphrodite between 120 and 150 m asl (Fig. 10a). Mc-1 documents a glacier whose main fronts reached the entrance to the north and east valleys, probably at least ~3 km downglacier of the 1962 front (Fig. 9).

Mc-2 is developed over ~1.4 km between the north and east valleys. Mc-3 and Mc-4, the best-preserved sets of moraines, can be followed more or less continuously over ~3.5 km, from the north-east area of the complex to the frontal moraine of Cirque West (Fig. 9). They are a combination of a few long- and many short-accreted moraines, ~50–100 m wide in the north-west area of the complex and up to ~200 m wide in the north-east area. They are ~5–10 m high, except the ~200 m-long central

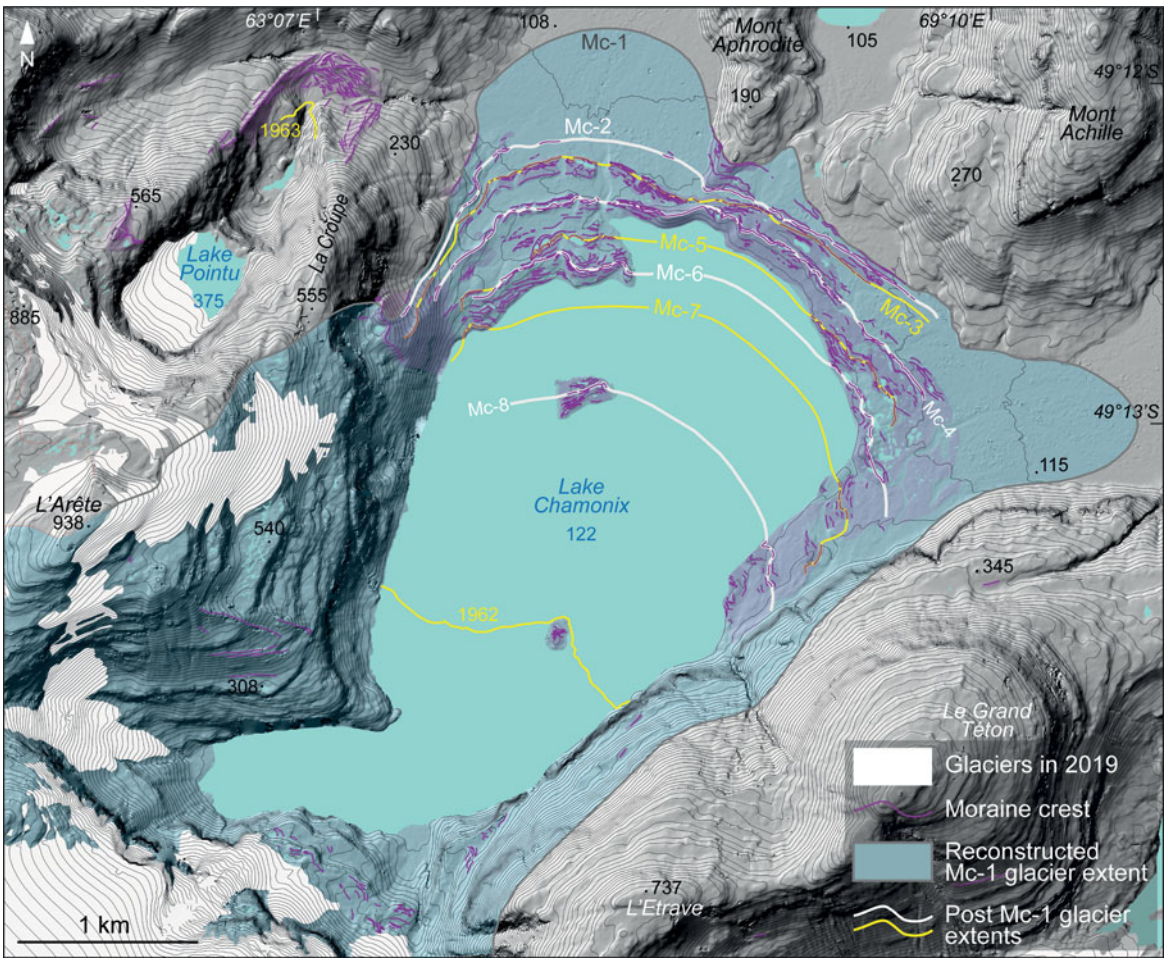

Figure 9. Chamonix Glacier morainic complex, with Mc-1 to Mc-8 moraine sets and the 1962 front position. Note the Pointu Glacier morainic complex to the north-west. Light purple = moraines. Topographic map from Pléiades-derived digital elevation model; contour interval: 10 m; elevation point in metres above sea level.

https://doi.org/10.1017/S0954102023000378 Published online by Cambridge University Press

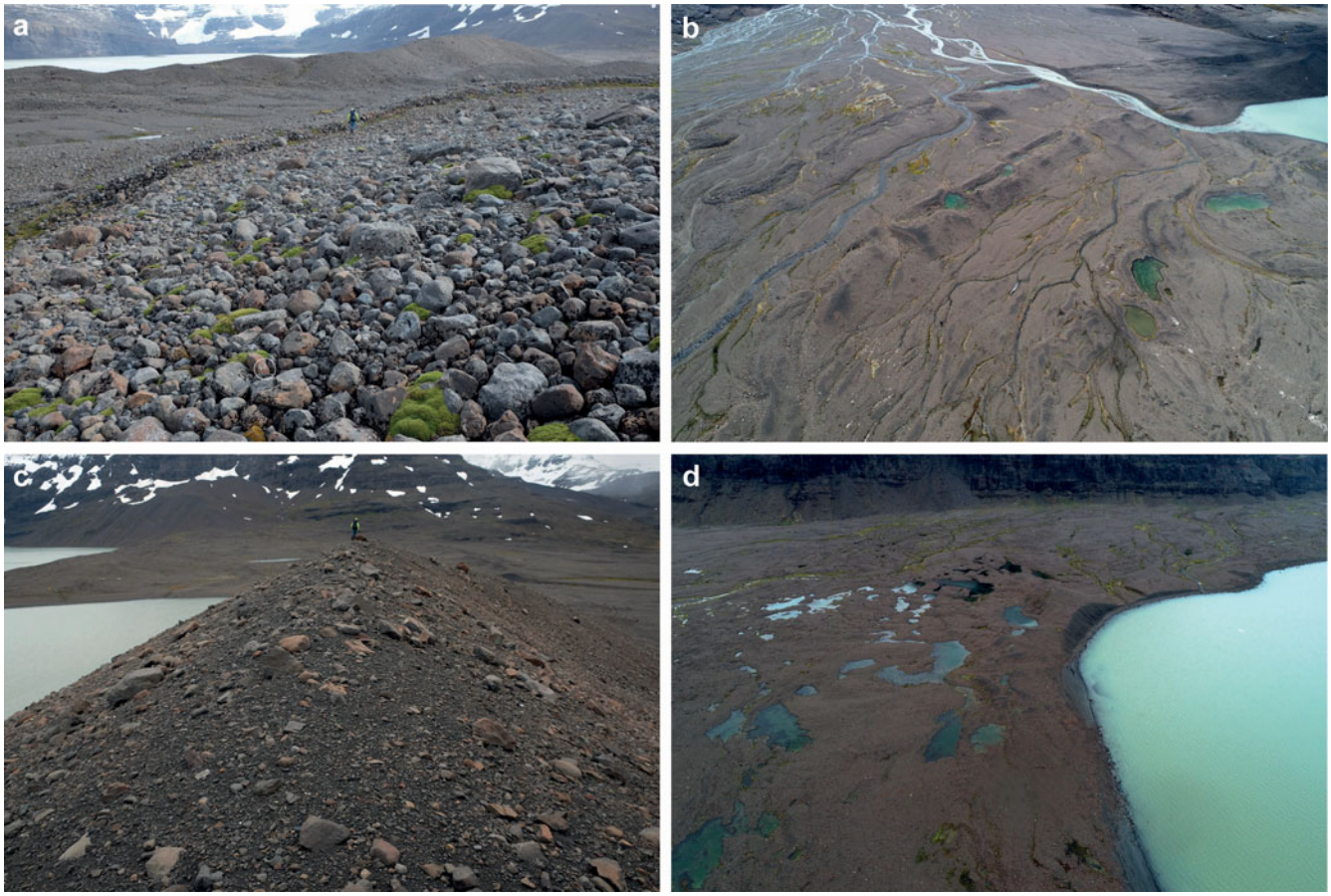

Figure 10. a. Northward view of bouldery sheet and lowest frontal moraine Mc-1 at the foot of the south side of Mont Aphrodite. Chamonix lake and glacier are in the background. Note on the right the 36 m-high frontal moraine Mc-4, which hides the lake. **b.** Eastward view of frontal moraines Mc-1 and Mc-2 on the left, Mc-3 in the middle and Mc-4 on the right, divided by the Lake Chamonix outlet river. **c.** Top of a 36 m-high section of moraine with matrix-supported till Mc-1. Moraines of Cirque West and the western end of Mc-1 to Mc-3 moraines in the background on the left. **d.** Eastward view of the eastern end of latero-frontal moraines Mc-5 on the left, Mc-6 along the lakeshore and Mc-7 in the background on the right.

section of Mc-4, which was probably built by a superposition that is 36 m high (Fig. 10c). The Mc-4 glacier front was ~2.3 km downglacier from that of 1962.

Mc-5, Mc-6, Mc-7 and Mc-8 are discontinuous. Mc-5 and Mc-6 are well developed on both the north-west and east sides of the lake (Fig. 10b,d), Mc-6 dominates the lake by ~19 m at its maximum height. Mc-7 and Mc-8 are only small moraines preserved on the lakeshore and the main island. Several > 100 m-long lateral moraines deposited on the south slope of Arête, 20–100 m above the 1962 glacier surface, possibly correspond to Mc-7 and Mc-8. The Mc-8 glacier front was ~1.2 km downglacier from that of 1962.

No moraines relate to the 1962 extent (Fig. 9). A few small ones were deposited in the following decade on the southern island and at the base of the east face of Etrave and, since the 1990s, in front of the retreating glacier at between 180 and 250 m asl (Fig. 9).

A total of 410 small lakes have been trapped in the intermorainic depressions, especially in the eastern area of the complex, the largest extending over ~2500 m^2 (Fig. 10d), and 125 others are present on the scoured ledges and flats of the south-east face of Arête (Fig. 9).

Smaller glacier forelands and morainic complexes

Mermoz Glacier has few moraines preserved, mainly after 1963, such as the ~20 m-high frontal moraine that dams Lake Mermoz. Two stages prior to 1963 can be distinguished. Two small complexes perched at ~450 m asl are related to cirque or slope glaciers (Fig. 11).

The Forel morainic complex comprises sub-concentric sets of numerous latero-frontal moraines extending over ~1 km^2, with four main stages from before 1962 (Fig. 11). Numerous lakes cover ~10% of this area. The outermost ~10 m-high frontal moraines, partly dismantled and whose bases are buried by the outwash

https://doi.org/10.1017/S0954102023000378 Published online by Cambridge University Press

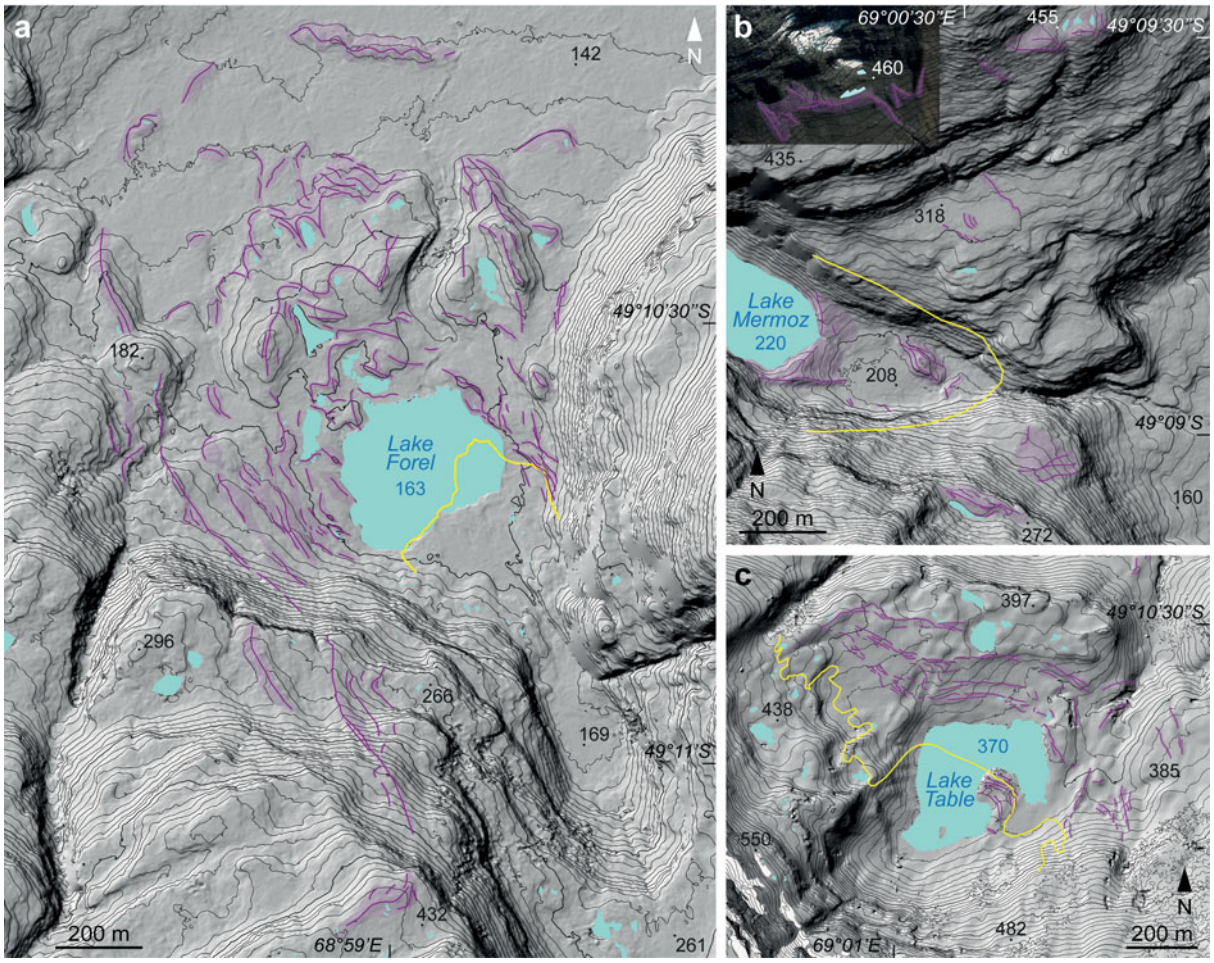

Figure 11. a. Forel, **b.** Mermoz and **c.** Table glacier morainic complexes. Light and dark purple = moraines and their crest lines, respectively; white = glaciers in 2019; yellow line = front position in 1962 (Mermoz Glacier: 1963). Google Earth orthoimage from 2015 is in the top-left corner of the Mermoz map to show the hanging glacier. Topographic map from Pléiades-derived digital elevation model; contour interval: 5 m; elevation point in metres above sea level.

plain, delimit a piedmont lobe whose front was ~950 m downglacier from that of 1962; a succession of left-lateral moraines ascend 300 m higher on the slope. One of the main sets of recessional moraines was probably deposited on several 25 m-high rocky hills that are not fully eroded by the glacier, closing the glacier-bed overdeepening; located in it, Lake Forel (0.08 km^2) is dammed by moraines built prior to 1962. Almost no moraines have been deposited since 1962. All recessional sets are incised by a > 50 m-wide and > 10 m-deep meltwater channel (Fig. 11).

Table Glacier has built at least three sets of 1 m-high pre-1962 frontal moraines in its cirque around Lake Table (0.1 km^2), probably flowing down to ~320 m asl through the eastern gorge at its maximum extent. Small moraines were deposited on the lake peninsula in the early 1960s (Fig. 11).

Lune Cirque shows an upper set of frontal moraines with a larger latero-frontal group that was probably deposited in the early 1960s (Fig. S8a) and several latero-frontal ones ~100–200 m downstream (Fig. 5).

Pointu Glacier was once an outlet glacier from the CIC that overflowed the Arête and incised the valley to the west of the lake, within which only a few moraines are now preserved (Fig. 9). Pointu morainic complex is composed of 1) subconcentric frontal moraines deposited downstream of a deep U-shaped valley, below Lake Pointu (0.1 km^2) and within 400 m of the 1962 front, and 2) two lateral moraines that ascend up to 300–350 m asl. No moraines have been deposited since 1962, and the two overdeepenings are now occupied by lakes (Figs 9 & S8b–d).

The reconstructed extent of Guynemer, Agassiz and Chamonix glaciers prior to the 1960s

A maximum extent (Mx-1) for each of the Guynemer, Agassiz and Chamonix glaciers in our study area has

https://doi.org/10.1017/S0954102023000378 Published online by Cambridge University Press

been reconstructed using their outermost set of preserved moraines noted in the field and by remote sensing. However, fjords, U-shaped valleys, overdeepenings filled by present lakes, roches moutonnées and erratic boulders that constitute the landscape downstream of these outermost moraines demonstrate that ice cover has been even more extensive in the past, but how far and how many times they advanced remain unknown. Six to nine subsequent advances have been reconstructed for each of the three glaciers.

The Mg-1 surface area of Guynemer Glacier (Fig. 3) was ~6.2 km^2. The glacier received ice from a Forel/Louise Glacier filling the overdeepened Louise Valley, of which Table and Mermoz glaciers were tributaries. As demonstrated by the orientation (330°N to 10°N) of roches moutonnées (especially on trachytic sills) and glacial grooves, Forel/Louise Glacier flowed over Col Louise into the Guynemer basin. Therefore, the limit of Mg-1 Guynemer Glacier in Fig. 3 in the area of Col Louise is only indicative. According to our modelling results, the maximum thicknesses of this 5 km-long glacier was 290 m into the Guynemer Glacier bed overdeepening (Fig. 12).

While the Forel/Louise Glacier still contributed over Col Louise, the Guynemer Glacier perfectly occupied the lower overdeepening at Mg-2, with a front ~500 m away from that of Mg-1. Mg-3, the first of four recessional moraine sets deposited between the lower and upper basins before the 1960s, highlights the dramatic retreat since Mg-2 was deposited (> 1.5 km). At the same time, Forel Glacier was probably confined to Louise Valley as it could not overflow through Col Louise. With a front 1.6 km away from that of Mg-2, the surface area of the glacier at Mg-3 was 55% of that of Mg-1. From Mg-3 to Mg-6, the glacier front retreated only to a distance of 400 m. After a further withdrawal of 235 m, Guynemer Glacier's surface area in 1963 was 45% of that of Mg-1.

The Ma-1 surface area of Agassiz Glacier was 38.2 km^2 (Fig. 5). Lune Glacier was a tributary from its left side, but the smaller glacier probably present in the cirque to the north probably was not. On its right margin, Agassiz Glacier flowed over both Plateau Hera and the ridge that extends from Mont Agassiz to the north-east, probably reaching the depressions now filled by lakes Athena and Hera. The maximum modelled thickness of this 14 km-long glacier reached 410 m (Fig. 12).

At Ma-2, the glacier front had retreated by only ~250 m. Plateau Hera had become largely ice-free, with ice no longer flowing through the Hera Pass. Nonetheless, ice was still probably flowing towards the east and Lake Athena, as suggested by an isolated, 100 m-long moraine standing ~5 m above the present shore of the lake (Fig. S3). After the front withdrew at least 700 m upstream of Ma-2, six subsequent glacier standstills were reconstructed before 1964, from Ma-3 to Ma-5, whose 250–300 m-wide set of frontal moraines have dammed Lake Agassiz north, to Ma-7 that dammed Lake Agassiz east (Fig. S3). The Agassiz Glacier extent at Ma-3 was still 57% of that of Ma-1. After its withdrawal of ~300 m from Ma-7 in 1964, its surface area was still 71% of that of Ma-1. Finally, Ma-9 moraines were deposited shortly before 1991, and Ma-10 moraines were probably deposited in 2000.

The Mc-1 surface area of Chamonix Glacier was 27.8 km^2 (Fig. 9). Two main lobes entered into the north and east valleys, ~1.25 and 0.75 km wide, respectively, with a minor one towards Lake Aphrodite. The east face of Arête was ice-covered, whereas the Mc-1 glacier surface was 150–200 m above the 1962 one on the west face of Etrave-Grand Téton (Fig. 9). The glacier-bed overdeepening presently occupied by Lake Chamonix probably extends into the north and east valleys, as suggested by the absence of a rocky sill at their entrance. The maximum modelled thickness is 620 m for the 8.8 km-long Mc-1 glacier (Fig. 12).

The front of Mc-2 Chamonix Glacier at the entrance of the north valley was ~600 m upstream of its Mc-1 position, whereas the Mc-2 surface area was still 95% of that of Mc-1. Subsequently, five recessional moraine sets (Mc-3 to Mc-7) were deposited over a distance of < 800 m, completed by Mc-8 as suggested by the moraines on the northern island. The small innermost moraines on the lake's eastern shore and the ~1.2 km distance between Mc-8 and the southern island where the 1962 front was grounded suggest that other standstills occurred in the meantime. The Chamonix Glacier extent in 1962 was still 62% of that of Mc-1.

The mean surface area of the three glaciers at the onset of the 1960s was still 65% of that of the Mx-1 stages. The ELAs were located at 385, 592 and 594 m asl for Guynemer Mg-1, Agassiz Ma-1 and Chamonix Mc-1, respectively (Fig. 12).

Surface area, front position and volume changes of glaciers since 1962

Glacier extent in the study area have been reconstructed for 12 time slices from 1962 to 2019 (Fig. 13), along with changes in the glacier front positions until 2021 (Fig. 14 & Table II). Fewer reconstructions were possible for Guynemer and Mermoz glaciers due to a lack of data, and there were even fewer data for the smaller Table and Lune glaciers.

The rate of glacier shrinkage has varied over this ~60 year period, partly driven by the type of front, either lake or land terminating. The retreat rate of the fronts was in the range 40–60 m a^{-1} from the 1970s to the 1990s, and this then decreased to 5–15 m a^{-1} during the last 25 years, excepted at Agassiz (~100 m a^{-1}) and

https://doi.org/10.1017/S0954102023000378 Published online by Cambridge University Press

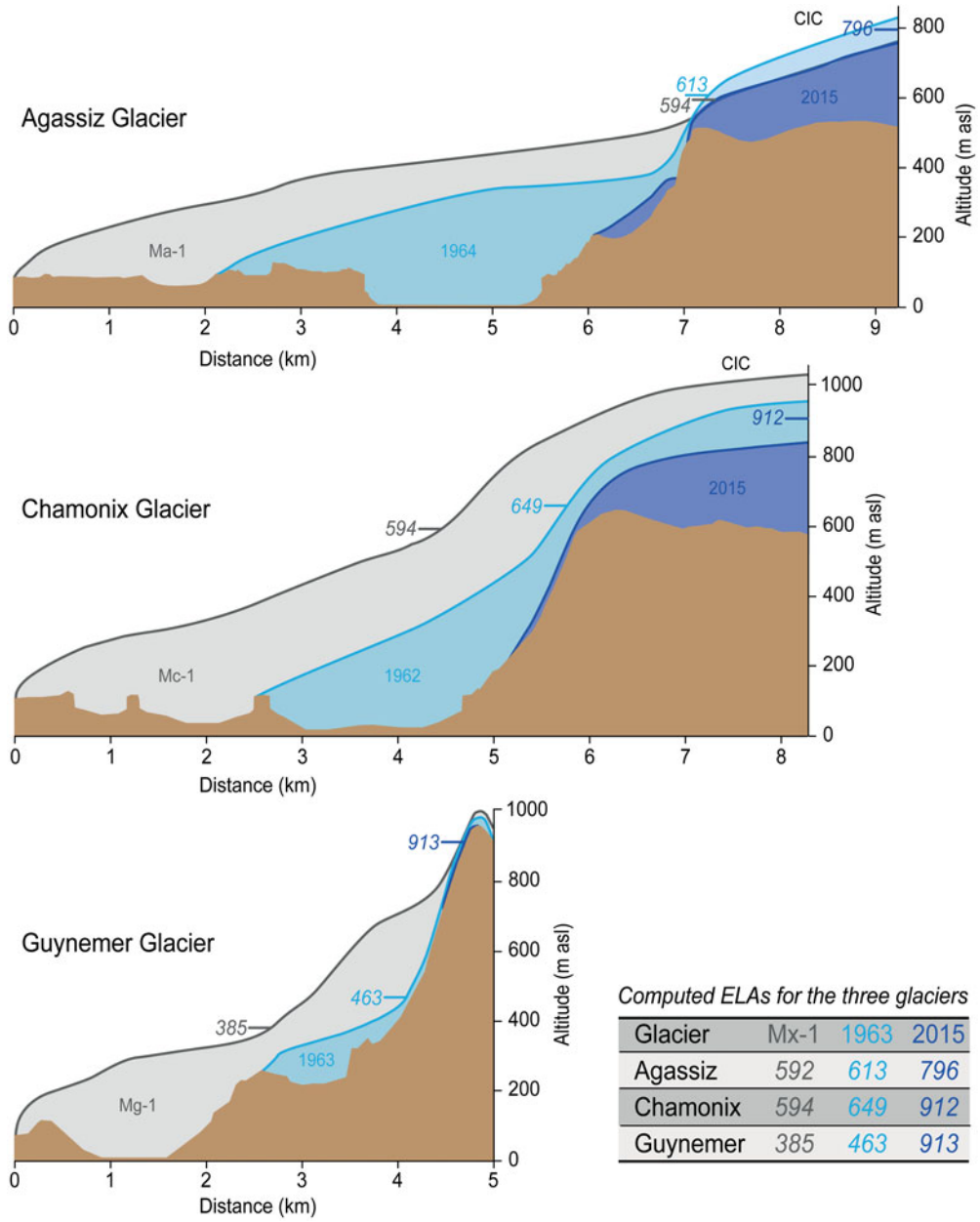

Computed ELAs for the three glaciers

Glacier	Mx-1	1963	2015
Agassiz	*592*	*613*	*796*
Chamonix	*594*	*649*	*912*
Guynemer	*385*	*463*	*913*

Figure 12. Reconstructed longitudinal profiles of Agassiz, Chamonix and Guynemer glaciers for Mx-1 stages (light grey), 1962–1964 (light blue) and 2015 (2019 for Guynemer Glacier; dark blue), with the respective computed equilibrium-line altitudes (ELAs) in italics (see text for methods used; 2015 ELAs of Agassiz and Chamonix glaciers are upstream of the profiles). 3.7× vertical exaggeration. Ma-1 profile, which should be above the two other profiles in the Cook Ice Cap sector, must therefore be considered with caution. m asl = metres above sea level.

Mermoz glaciers (Fig. 14). Attenuated, the retreat rate of the glacier surface areas has been rather constant since the 1960s (e.g. ~0.1 km^2 a^{-1} for Chamonix), except at Agassiz, where it increased to ~0.5 km^2 a^{-1} since the 1990s (Fig. 14).

The fronts of Forel and Table glaciers were already lake-based in 1962, so calving accelerated their retreat (Benn *et al.* 2007). As the Chamonix Glacier front was partly grounded on an island, it was still close to its 1962 position in 1971, although its surface area had decreased by more than 1 km^2 (Fig. 9a); once the glacier lost this grounding, its shrinkage accelerated.

The data gap between 1971 (or even 1962–1963 for several glaciers) and 1991 does not allow for the detailed reconstruction of the glacier dynamics during this 20–30 year period. In 1991, the front of Chamonix Glacier became land-based, unlike the Guynemer and Mermoz glaciers, which had only retreated from the

https://doi.org/10.1017/S0954102023000378 Published online by Cambridge University Press

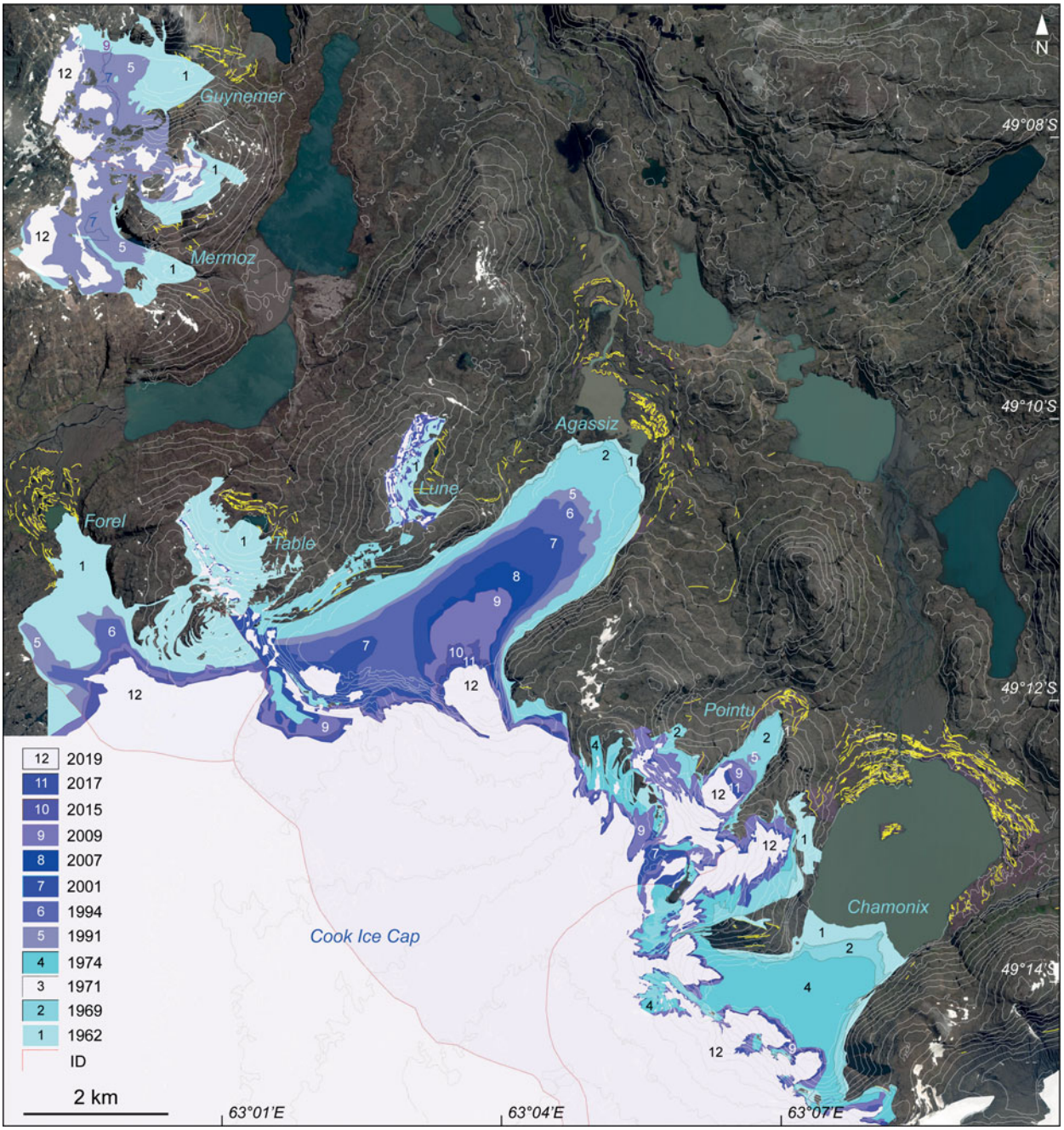

Figure 13. Glacier extents from 1962 to 2019. Yellow = moraine crest lines. Some extents are only represented by their front (e.g. 2015 at Pointu; 2001 and 2009 extents at Guynemer are labelled on the map). ID = ice divide in 1962. Pléiades orthoimage from 2021 (Bing Aerial); contour interval: 50 m.

downstream area of their overdeepening, occupied by the growing lakes. Still land-based, the Pointu Glacier front overflowed from the upper overdeepening and fed a small regenerated glacier in 1991. Its front remained stationary from 1994 to 2009, then became lake-calving, accelerating its retreat (e.g. 250 m from 2015 to 2021).

In 1973, the front of Agassiz Glacier was still at its 1971 position, ~150 m upglacier of its 1964 position, as shown on a declassified US airborne image from 28 April. Ma-9 moraines were deposited shortly before 1991. The northern end of the present Lake Agassiz north became ice-free in 1991, but the glacier still occupied the wide overdeepening with its surface at least 100 m higher than the present lake level (Fig. S9b). Due to its firm grounding, it did not become water-terminating until the early 2000s, as demonstrated by a 15 m-resolution

https://doi.org/10.1017/S0954102023000378 Published online by Cambridge University Press

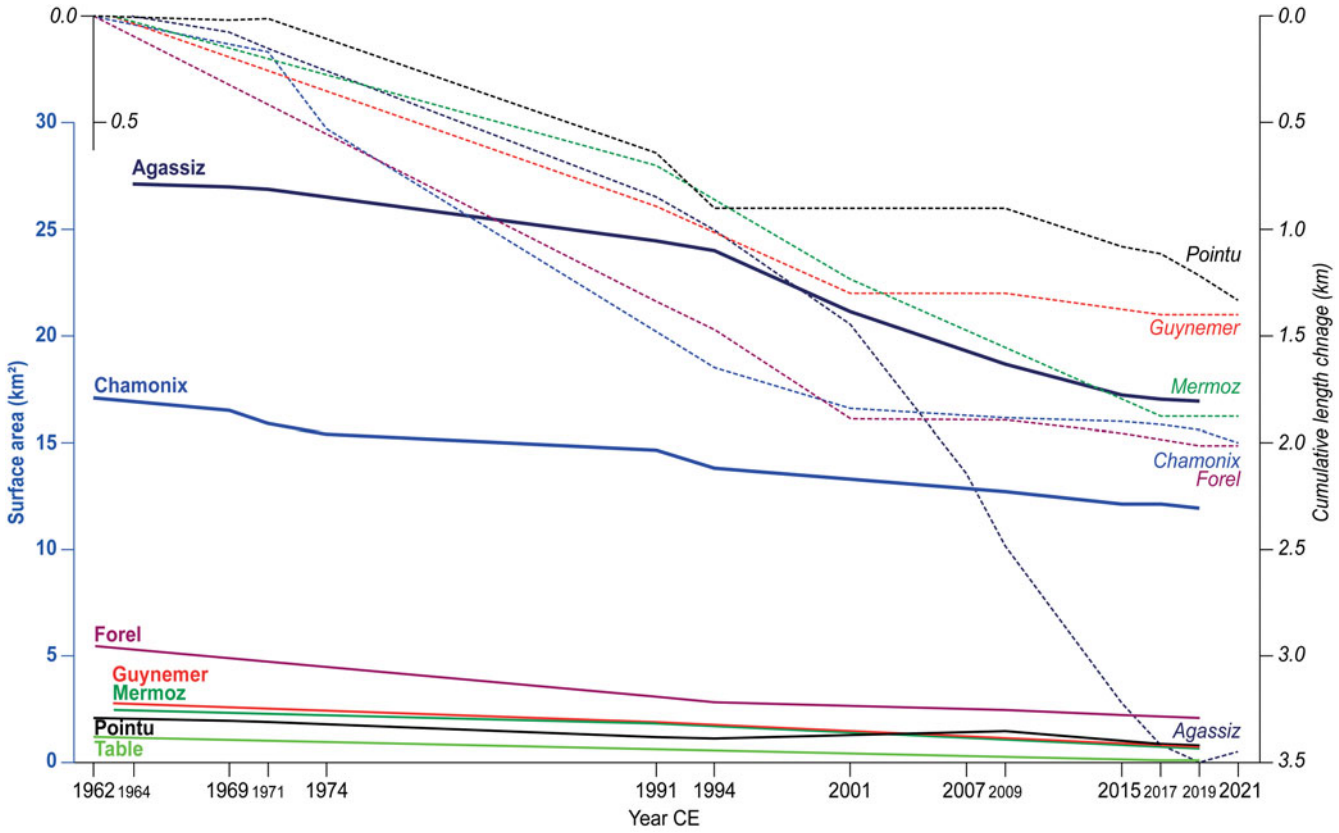

Figure 14. Changes of glaciers north-east of Cook Ice Cap. Surface area change from 1962 (1963 for Guynemer and Mermoz, 1964 for Agassiz) to 2019 for seven glaciers (solid lines, blue *y*-axis) and cumulative length change from 1962 (1963, 1964) to 2021 for six glaciers (dashed lines, black *y*-axis). See Table II for data.

ASTER image from 12 January 2000 depicting that the front was still reaching the rock cap in the northern area of the lake, where it probably deposited the small Ma-10 moraines (Fig. 5). A Landsat image (Table I) taken on 27 November 2001 shows that the front had retreated by ~60–150 m in < 2 years and Lake Agassiz south had begun to form. The front rapidly retreated by ~2 km in the following decades (Fig. 14).

The retreat of the studied glaciers resulted in negative cumulative length changes from 1962 to 2021: < 1.5 km for Pointu and Guynemer glaciers, ~2 km for Mermoz, Chamonix and Forel glaciers and 3.5 km for Agassiz Glacier (Fig. 14 & Table II). Finally, as shown by Bing Satellite images, the Agassiz and Chamonix (northern) fronts have retreated by ~140 and 40 m between 2021 and 2022, respectively, with the two other fronts of Chamonix being stationary.

In 2019, the total surface area of the eight glaciers was only 56.5% of that of 1962, with variations between glaciers: Guynemer and Mermoz glaciers have each lost ~74.0% of their surface areas, as opposed to 30.6% and 37.6% for Chamonix and Agassiz glaciers, respectively, and 43.5% for the eight studied glaciers. While the Forel and Pointu glaciers lost approximately two-thirds of their areas, Table and Lune glaciers had probably vanished by 2015, as suggested by slight annual changes of the patchy snowpack covering ice remnants. The shrinkage has less impacted the CIC outlet glaciers, as ~75% of the surface area of the entire CIC was still > 600 m asl in 2009 (Verfaillie *et al.* 2015).

The volume change of Chamonix Glacier since the 1960s was computed by taking into account both the assessed bathymetry of Lake Chamonix and the bedrock topography below the CIC obtained with *GlabTop*. The volumes of the glacier were 1.96 and 0.96 km^3 in 1962 and 2019, respectively, representing an ice volume loss of 1.0 km^3 (Fig. S10).

Equilibrium-line altitudes since the 1960s

The MELM was used to estimate the ELA (e.g. Torsnes *et al.* 1993) during the 1960s. This method gives an approximate estimate of the ELA, as the debris transported from the accumulation zone is deposited on the margins of the ablation zone, below the ELA. According to the MELM, the highest lateral moraines probably deposited at the onset of the 1960s suggest that the minimum ELA would have been at 700 m asl at

https://doi.org/10.1017/S0954102023000378 Published online by Cambridge University Press

Table II. Surface area and change of length of the eight glaciers in our study area from 1962 to 2021. Italics = cirque glaciers; bold = outlet glaciers from Cook Ice Cap; regular font = glacier outside of the study area.

	1962	1969		1971		1974		1991		1994		2001[a]	2007	2009		2015		2017		2019		2021[b]
No. in Fig. 13	1	2		3		4		5		6		7	8	9		10		11		12		
Glacier	A (km^2)	A (km^2)	ΔL (km)	A* (km^2)	ΔL (km)	A (km^2)	ΔL (km)	A (km^2)	ΔL (km)	A (km^2)	ΔL (km)	A (km^2)	ΔL (km)	ΔL (km)	A (km^2)	ΔL (km)	A (km^2)	ΔL (km)	A (km^2)	ΔL (km)	A (km^2)	ΔL (km)	ΔL (km)
Guynemer	*2.80*[c]							*1.90*	*-0.89*				*-1.30*			*-1.30*				*-1.40*	*0.72*	*-1.40*	*-1.40*
Mermoz	*2.62*[c]							*1.91*	*-0.70*				*-1.24*							*-1.87*	*0.70*	*-1.87*	*-1.87*
Forel	**5.58**							**3.21**	**-1.34**	**2.83**	**-1.47**		**-1.88**		**2.48**	**-1.89**	**2.28**	**-1.95**			**2.12**	**-2.07**	**-2.07**
Table	*1.26*																	*nr*	*0.15*	*nr*	*0.14*	*nr*	*nr*
Lune	*0.65*[c]																*0.35*	*nr*	*0.14*	*nr*	*0.12*	*nr*	*nr*
Agassiz	**27.15**[c]	**26.93**	**-0.07**	**< 26.9**	**-0.16**			**≤ 24.4**[d]	**-0.84**	**≤ 24.0**[d]	**-1.02**	**21.15**	**-1.45**	**-2.14**	**18.68**	**-2.48**	**17.25**	**-3.22**	**17.06**	**-3.42**	**16.93**	**-3.50**	**-3.46**
Pointu	*2.04*	*1.96*	*-0.02*	*< 1.9*	*-0.01*			*≥ 1.21*[d]	*-0.64*	*1.14*	*-0.90*		*-0.90*		*1.37*	*-0.90*		*-1.08*	*0.82*	*-1.14*	*0.71*	*-1.22*	*-1.33*
Chamonix	**17.16**	**16.56**	**-0.13**	**< 16.0**	**-0.17**	**15.45**	**-0.53**	**≤ 14.7**[d]	**-1.48**	**≤ 13.8**[d]	**-1.65**		**-1.84**		**12.70**	**-1.88**	**12.21**	**-1.90**	**12.17**	**-1.92**	**11.90**	**-1.94**	**-2.00**
Total	59.26																				33.49		
Ampère	**82.2**[e]				**-0.02**[f]			**72.4**[e]	**-1.80**[e]		**-1.85**[e]	**66.8**[e]		**-2.83**[e,g]	**61.5**[h]			**-3.28**[b]					**-4.27**

TAAF flight surveys took place during summers, straddling 2 years; for the sake of simplicity, we use the first year in the reference number of the aerial images (e.g. 1962 for 1962–1963; see Table I).
Length change is measured along the shortest distance from the 1962/1963/1965 front, except for Pointu Glacier since 2015 (distance to the centre of its concave-shaped front) and Mermoz Glacier (due to the curvature of the glacial trough). The shape and/or discontinuity of the smallest glaciers (Table and Lune glaciers) in the recent years do not allow for length change measurement.
Surface area change integrates all areas of the glacier, even those disconnected from the main tongue, contrary to Randolph Glacier Inventory (RGI) 6.0 (https://doi.org/10.7265/4m1f-gd79).
Guynemer and Mermoz glaciers in 1962: because of the snowpack that year, we used 1963 images.
Lune Glacier in 1962: as no aerial image is available in 1962, we used a 1964 image.
Agassiz Glacier in 1962: as no aerial image covers its distal area for that year, this was delineated from a 1964 image.
Chamonix Glacier in 1962: as the aerial image only covers its distal area that year, the upglacier area was delineated from a 1964 image.
Agassiz Glacier in 1969: as no aerial image covers the upper basin/Cook Ice Cap for that year, this was delineated from a 1962 image.
Chamonix Glacier in 1969: bedrock 'windows' (Les Hublots) in the upglacier area were delineated from a 1969 Frölich oblique aerial image (fig. A+C).
Guynemer and Mermoz glaciers in 1991: because of the snowpack (September), upglacier areas were delineated from 1964 images.
Agassiz Glacier in 2019: except for its front, this was delineated from the 2017 image due to cloud cover.
[a]Landsat 2001/2011.
[b]Bing Aerial 2021.
[c]1963 or 1964.
[d]Computed from the distal area only.
[e]Berthier *et al.* (2009).
[f]Vallon (1977a).
[g]2006.
[h]Cogley *et al.* (2014).
A = surface area; A* = estimated surface area; ΔL = length change; nr = non-representative.

Chamonix, ~600 m at Pointu, ~550 m at Agassiz, ~450 m at Forel and 425 m at Guynemer glaciers. The ELAs computed from our reconstructed 1960s extents of Chamonix (649 m), Agassiz (613 m) and Guynemer (463 m) glaciers are close to the ELAs estimated using the MELM method (Fig. 12).

As the ELA may coincide with the transient snowline (i.e. the lower limit of snow on the glacier at the end of the ablation season), it can be identified from satellite and aerial images for certain years (Rabatel *et al.* 2013). However, the precise dates of the aerial images between 1962 and 1974 are unknown, and satellite images since 1991 have rarely been taken in February or March (Table I). The snowline on Agassiz Glacier was between 620 and 700 m asl in March 1994, ~600 m in March 2001 (Verfaillie *et al.* 2015, fig. 6) and up to 800 m in March 2017 and 750 m in 2021. Besides their inter-annual variability, these snowline elevations approximately match with the ELA of ~800 m computed from the reconstructed 2015 Agassiz extent (Fig. 12). Contemporaneous ELAs for Chamonix and Guynemer glaciers were higher, at ~900 m asl (Fig. 12).

Lake dynamics since the 1960s

Among the 2636 lakes of > 1 m^2 present in our study area in 2019, 1128 appeared since 1962 due to the glacier shrinkage, whereas the already-existing lakes Forel, Table, Agassiz east and Chamonix increased in size. The post-1962 lakes are generally small except lakes Guynemer, Mermoz, Agassiz south and Pointu, whose total surface area of 1.93 km^2 represents 89% of that of the post-1962 lakes, but only 9% of the surface area of all lakes. Lake Chamonix increased in size by 37% between 1962 and 1991, from 4.15 to 5.68 km^2.

High summer turbidity in the fjords, lakes and rivers, especially when directly connected to a glacier, demonstrates the intensity of the glacial and paraglacial erosion in the region (Fig. 2). The colour of the lakes (a proxy of their suspended sediment load) varies as to whether or not they are fed by glaciers as a first-order factor (Giardino *et al.* 2010, Matta *et al.* 2017). Lakes that have not been glacier-fed for an extended period of time, such as lakes 5a or 6, have the lowest turbidity, similar to Lake Aphrodite, which Chamonix Glacier has intermittently fed with glacial meltwater. Since Lake Surprise acts as a sediment trap, Lake Guynemer also appears blue in colour, in contrast with the brown colour of lakes Agassiz south and north, which were ice-filled or close to the glacier front < 25 years ago. The water level of some lakes fluctuates throughout the year (Fig. S11). Waves generated by stormy winds produce ~1–2 m-high stepped profiles with several berm crests on pebble beaches, for instance, on the north shores of lakes Chamonix and Aphrodite.

Discussion

Limitations in our reconstruction of the glacier stages before the 1960s

Besides the limitations discussed earlier in the 'Methods' section, there are others that also affect our reconstructions to varying degrees. As the preservation of moraines depends on composition, initial size, weathering and erosion, geomorphic evidence of past glacier extents can vanish quickly. The Agassiz and Chamonix stages have been reconstructed by connecting existing moraines that are generally discontinuous, which introduces uncertainties. Moreover, the Mc-1 front of Chamonix Glacier is poorly constrained, as corresponding moraines are few and even absent in the north and east valleys filled with sandurs (Fig. 9). By contrast, the Guynemer and Agassiz areas have narrow valleys and preserved terminal moraines. The margins of Mx-1 in the upper basins are generally not constrained by moraines or trimlines: in the Surprise basin, for instance, Mg-1 outlines remain ambiguous, except when in correspondence with the summit ridge (Fig. 3). The outlines of Mx-1 in the three upper basins are therefore based on glaciologically 'reasonable' assumptions.

The contribution of Forel/Louise Glacier to the ice flowing into the Guynemer basin should be integrated to assess the characteristics of Mg-1 and probably Mg-2 in a more robust way (Fig. 3), and the ice cover resulting from *GlaRe* is incomplete on the slopes (Fig. 12).

Finally, reconstruction before the 1960s is proposed for only three glaciers, limiting the analysis of glacial dynamics.

Comparing glacier extents before the 1960s in our study area with those elsewhere in Kerguelen

Similar to Ampère and Arago glaciers, many of the moraine sets of the Guynemer and Agassiz glaciers predating the 1960s do not exceed the glacier position of 1962 by > ~1 km, which is even more so the case for the smaller glaciers such as Forel or Pointu. There are larger distances for the Chamonix moraines probably because their retreat was accelerated due to calving, which slowed down later when the front became grounded on the southern island. Well-preserved moraine sets > 2 km downglacier of the 1962 front are present in the Agassiz and Chamonix forefields, which is only the case with Gentil Glacier amongst the previously studied glaciers of the archipelago. However, a mean 2.6 ka age of the debris-covered icy ridge at the Gentil front (Charton *et al.* 2020) shows that debris-covered glacier dynamics differ from those of clean-ice glaciers.

Glaciers have significantly carved the landscape downstream of Mx-1 down to the Baie du Repos, as shown by the deep overdeepening of this fjord (-175 m

https://doi.org/10.1017/S0954102023000378 Published online by Cambridge University Press

asl at its maximum) and the large erratic boulders along its shores. But contrary to Arago Glacier and Val Travers and Bontemps areas, where frontal moraines are deposited 11–25 km downglacier of the present glacier fronts, no other moraine sets are present in our study area. However, a greater glacier extent prior to Ma-1 is suggested by 1) three moraines deposited just outside the distal right-latero-frontal moraine of Ma-1 and 2) small moraines probably protruding from the sandur and alluvial fans ~350–600 m downstream of the Ma-1 frontal moraines (Fig. 2).

Moraine types and dynamics in the study area

There is an irregular distribution of moraines according to their type (clast-supported *vs* matrix-supported tills) within the discussed complexes. The dominance of moraines with matrix-supported till in the downstream area of glacier forelands (Mg-1 and Mg-2 at Guynemer, Ma-1 to Ma-8 at Agassiz) could result from the debris comminution related to the duration of active glacier transport (Boulton 1978), whereas boulders abundant in moraines with clast-supported till in the upstream areas of forelands (Mg-3 to Mg-6 at Guynemer, Ma-4 to Ma-6 at Agassiz) could have been supplied by rockfalls during periods prone to glacial debuttressing or permafrost degradation. At Chamonix foreland, however, Mc-1 is formed with clast-supported till, whereas later morainic sets of the complex are composed of matrix-supported till.

Another characteristic of many frontal moraines in the study area is their low height of ~5–10 m. This partly results from the thick glacifluvial sediments of the outwash plain that bury the base of the moraines at Agassiz and Chamonix forelands. On the other hand, large sub-angular boulders of a metric size scattered on the proximal side and top of the ~10 m-high smooth Ma-2 frontal moraines (Figs 8b & S5c) or sub-angular to sub-rounded boulders of a metric size littering the Ma-1 surface (Fig. 8c) suggest a post-glacial erosion.

Accelerated mass loss of lake-terminating glaciers since 1962

Lake-terminating glaciers generally experience a faster retreat than land-based ones, as shown in Greenland from 1900 (Carrivick *et al.* 2023), the Southern Alps (New Zealand) from the 1980s (Carrivick *et al.* 2022), Sikkim Himalaya for 2000–2010 (Basnet *et al.* 2013), Central Himalaya for 2000–2015 (King *et al.* 2018) and on the Tibetan Plateau for 1990–2014 (Wang *et al.* 2017). Glacial retreat in the study area has been very rapid during their lake-terminating period, which was also the case for Ampere Glacier south of the CIC (Berthier *et al.* 2009): although the front was stationary during the 1960s when it was mainly land-based, its lake-terminating front retreated by ~4.3 km until 2021 (Table II).

King *et al.* (2018) suggest that lake-based glaciers experience three phases of shrinkage: 1) no change in the glacier dynamics during the onset of the lake expansion; 2) calving becomes active as the lake is growing, which leads to retreat acceleration, compensated by ice flow while lateral and basal drag diminishes (Benn *et al.* 2007); and finally 3) glacier thinning and enhanced drag in shallow water and valley narrowing decrease ice flow and retreat rates. The retreat dynamics of Agassiz Glacier followed this pattern (Figs 13 & 14 & Table II): the land-based front was stationary between 1965 and the end of the 1980s; then the lake-terminating phase 1 showed a slow retreat (~600 m) during the 1990s; phase 2 lasted until 2015 with a retreat of ~1900 m; henceforth land-based, the steep front retreated slowly, standing within 150 m of the lake shore in 2021.

Changes in ELAs since the maximum glacier extents

Our ELA modelling combined various data sources and approaches, which introduces uncertainties. Moreover: 1) the glacier bed with its complex bed features such as rock cliffs or overdeepenings makes it challenging to model ELA (Keeler *et al.* 2021); 2) the 'geometric' ELA rise resulting from the retreat of the CIC 'flat' outlet glaciers from Mx-1 to 1962 (Chamonix: ~60 m) or even to the beginning of the 2010s (Agassiz: ~110 m) is probably underestimated by the AAR method compared to the 'climatic' ELA rise; and 3) the ELA of water-terminating glaciers differs from the 'climatic' ELA.

Nevertheless, the ELAs and ELA depressions of our three glaciers are coherent enough to be discussed (Fig. 12). Guynemer Mg-1 ELA is ~200 m lower than Ma-1 and Mc-1 ELA, which either suggests that Mg-1 is at an older stage or that the dynamics of this mountain glacier differ from those of the CIC outlets. Similar ELAs for Ma-1 and Mc-1 suggest that these stages are contemporaneous, especially since their surface areas (~38 and 28 km^2, respectively) and the general shape and elevation of these CIC outlets are comparable. However, the *GlaRe* reconstruction of Ma-1 should be considered with caution as the corresponding glacier surface on the CIC is below that of the 1964 extent and similar to the 2015 extent (Fig. 12). Therefore, a greater thickness of the CIC for Ma-1 would result in a steeper glacier profile downstream of the rock cliff and a lower ELA.

The slight ELA rises in 1962 and 1964 for Chamonix and Agassiz glaciers compared to Mx-1 could result from the weakness of the AAR method for flat areas, but the ELA rise for Guynemer Glacier in 1963 also seems low despite its different topography (Fig. 12).

https://doi.org/10.1017/S0954102023000378 Published online by Cambridge University Press

However, these three ELAs at the onset of the 1960s are close to the MELM values. Finally, the ELA rise of 450 m at Guynemer between the 1960s and 2019 is dramatic, by contrast with those of Agassiz and Chamonix glaciers (180–260 m).

The dynamics of the glacier shrinkage can be related to the types of glaciers studied. Once a valley glacier, Guynemer Glacier then retreated into its cirque. Its dynamics therefore differ from those of the CIC outlet glaciers, which are much larger with wide and elevated accumulation areas. Moreover, Guynemer Massif probably acts as a barrier to the precipitation associated with the SWW, with less snow deposition on the leeside where Guynemer Glacier is located, whereas on the wind-exposed CIC windblown snow accumulates on the leeward side, which corresponds to the upper basin of the outlet glaciers of our study area. Nevertheless, all of the glaciers in the Guynemer-Chamonix region have been affected by changes in their long-term or more recent shrinkage dynamics, as they all have been lake-terminating glaciers at some point: Guynemer after Mg-2, Guynemer, Mermoz, Forel and Table in the 1960s, Chamonix until the 1970s and Agassiz until the beginning of the 2010s, whereas Pointu was still lake-based in 2021.

Conclusion

Well-preserved morainic complexes are present at Kerguelen in the area north-east of the CIC. Their detailed geomorphological study and mapping allowed for the reconstruction of two to eight glacier stages for each glacier before the 1960s. The cumulative length change from the Mx-1 stage to 1963 was higher for the larger glaciers (-3 km for Chamonix, -2.7 km for Guynemer, -2.1 km for Agassiz) than for the smaller glaciers (-1 km for Forel, -500 m for Table, -400 m for Pointu). Loss in surface area during this period was lower for Chamonix and Agassiz glaciers (-38% and -29%, respectively) than for Guynemer Glacier (-55%).

Glacier shrinkage has dramatically accelerated since the beginning of the 1960s. Front retreats range from 1.3 to 3.5 km, with a loss in surface area of between 31% (Agassiz) and 74% (Guynemer) and a mean value of 44% for the eight studied glaciers for the period 1962–2019. In 1962, the surface areas of Guynemer, Agassiz and Chamonix glaciers were still 45%, 71% and 62% of those of their maximum reconstructed extents (Mx-1), respectively. In 2019, their surface areas had decreased to 12%, 44% and 43% of Mx-1, respectively.

In agreement with the changes in the glacier dynamics from around the 1960s, the ELA rise increases dramatically at Guynemer Glacier (+450 m in the second period *vs* +80 m in the first period) and less so at Chamonix (+260 m *vs* +55 m) and Agassiz (+180 m *vs* +20 m) glaciers.

To utilize the moraine chronologies from Kerguelen as an archive of past climate and to make inferences regarding the state of the SAM over time, precise dating of the moraines and quantification of the impacts of precipitation and temperature on mass balance are required.

Supplemental material

A supplemental table and supplemental data file will be found at https://doi.org/10.1017/S0954102023000378.

Acknowledgements

Pléiades and SPOT images were acquired through the Integrated Software for Imagers and Spectrometers (ISIS) and Spot World Heritage (SWH) programmes of the CNES, respectively. Xavier Bodin (EDYTEM) is acknowledged for processing the DEM and orthoimage from the 2019 Pléiades images, and Etienne Berthier (LEGOS) is acknowledged for providing access to his DEM from the 2015 Pléiades images. Aart Verhage, Charline Giguet-Covex (EDYTEM) and Eivind N. Støren (BCCR) are acknowledged for their logistical assistance in the field. Pierre Sabatier (EDYTEM) is acknowledged for preparing the project PALAS. Institut Polaire Français (IPEV) has funded the project PALAS2 ('PAleoclimate from LAke Sediments on Kerguelen Archipelago 2'; project number: 1094); Yann Le Meur and the sub-Antarctic IPEV team are warmly acknowledged for the preparation and the logistical support in the field. The fieldwork for this paper is part of the Norwegian Research Council funded project 'Past behaviour of the Southern Ocean's atmosphere' (SOUTHSPHERE, 2016–2024; project number: 267719). We thank the two reviewers for their detailed comments that helped to improve the text. Finally, Cliff Atkins (editor) and Mariel Kieval (managing editor) are acknowledged for their responsiveness and John Marr (copyeditor) is thanked for his deep copyediting of the manuscript.

Authors contributions

FA and JB led the projects SOUTHSPHERE and PALAS2. PD, HL and LR conducted the geomorphological fieldwork, with the logistical assistance of FA and JB. PD mapped the morainic complexes and the 1962–2029 glacier extents. PD, HL, LR and TT conducted the geomorphological analysis. RL conducted the glacier thickness and ELA modelling. PD prepared the figures. PD, FA and JB wrote the draft. PD, HL, LR, TT, FA and JB edited the manuscript prior to submission.

Competing interests

The authors declare none.

References

Aubert de la Rüe, E. 1932. Etude géologique et géographique de l'archipel de Kerguelen. *Revue de la géographie physique et de géologie dynamique*, **5**, 231 pp.

Aubert de la Rüe, E. 1967. Remarques sur la disparition des glaciers de la Péninsule Courbet (Archipel de Kerguelen). *TAAF, La Documentation Française, Paris*, **40**, 3–19.

Bakke, J., Paasche, Ø., Schaefer, J., Paasche, Ø. 2021. Long-term demise of sub-Antarctic glaciers modulated by the Southern Hemisphere westerlies. *Scientific Reports*, **11**, 10.1038/s41598-021-87317-5.

Balco, G. 2020. Glacier change and paleoclimate applications of cosmogenic-nuclide exposure dating. *Annual Reviews of Earth and Planetary Sciences*, **48**, 10.1146/annurev-earth-081619-052609.

Basnett, S., Kulkarni, A.V. & Bolch, T. 2013. The influence of debris cover and glacial lakes on the recession of glaciers in Sikkim Himalaya, India. *Journal of Glaciology*, **59**, 10.3189/2013JoG12J184.

Bauer, A. 1963. Les glaciers de l'île de Kerguelen. *Comité National Français des Recherches Antarctiques*, **2**, 1–80.

Benn, D.I. & Gemmell, A.M.D. 1997. Calculating equilibrium-line altitudes of former glaciers by the balance ratio method: a new computer spreadsheet. *Glacial Geology and Geomorphology*, **1997**, 7.

Benn, D.I. & Lehmkuhl, F. 2000. Mass balance and equilibrium-line altitudes of glaciers in high-mountain environments. *Quaternary International*, 65–66, 10.1016/S1040-6182(99)00034-8.

Benn, D.I., Warren, C.R. & Mottram, R.H. 2007. Calving processes and the dynamics of calving glaciers. *Earth-Science Reviews*, **82**, 10.1016/j.earscirev.2007.02.002.

Berthier, E., Le Bris, R., Mabileau, L., Testut, L. & Rémy, F. 2009. Ice wastage on the Kerguelen Islands (49°S, 69°E) between 1963 and 2006. *Journal of Geophysical Research*, **114**, 10.1029/2008JF001192.

Boulton, G. 1978. Boulder shapes and grain-size distributions of debris as indicators of transport paths through a glacier and till genesis. *Sedimentology*, **25**, 10.1111/j.1365-3091.1978.tb00329.x.

Bryan, S.E. & Ernst, R.E. 2007. proposed revision to large igneous province classification. *Earth-Science Reviews*, **86**, 10.1016/j.earscirev.2007.08.008.

Carrivick, J.L., Boston, C.M., Sutherland, J.L., Pearce, D., Armstrong, H., Bjork, A., *et al*. 2023. Mass loss of glaciers and ice caps across Greenland since the Little Ice Age. *Geophysical Research Letters*, **50**, 10.1029/2023GL103950.

Carrivick, J.L., Sutherland, J.L., Huss, M., Purdie, H., Stringer, C.D., Grimes, M., *et al*. 2022. Coincident evolution of glaciers and ice-marginal proglacial lakes across the Southern Alps, New Zealand: past, present, and future. *Global and Planetary Change*, **211**, 10.1016/j.gloplacha.2018.05.006.

Chandler, B.M.P., Lovell, H., Boston, C.M., Lukas, S., Barr, I.D., Benediktsson, Í.Ö., *et al*. 2018. Glacial geomorphological mapping: a review of approaches and frameworks for best practice. *Earth-Science Reviews*, **185**, 10.1016/j.earscirev.2018.07.015.

Charton, J., Jomelli, V., Schimmelpfennig, I., Verfaillie, D., Favier, V., Mokadem, F., *et al*. 2020. A debris-covered glacier at Kerguelen (49°S, 69°E) over the past 15 000 years. *Antarctic Science*, **33**, 10.1017/S0954102020000541.

Charton, J., Schimmelpfennig, I., Jomelli, V., Delpech, G., Blard, P.-H., Braucher, R., *et al*. 2022. New cosmogenic nuclide constraints on Late Glacial and Holocene glacier fluctuations in the sub-Antarctic Indian Ocean (Kerguelen Islands, 49°S). *Quaternary Science Reviews*, **283**, 10.1016/j.quascirev.2022.107461.

Civel-Mazens, M., Crosta, X., Cortese, G., Michel, E., Mazaud, A., Ther, O., *et al*. 2021. Antarctic Polar Front migrations in the Kerguelen Plateau region, Southern Ocean, over the past 360 kyrs. *Global and Planetary Change*, **202**, 10.1016/j.gloplacha.2021.103526.

Cogley, J.G., Berthier, E. & Donoghue, S. 2014. Remote sensing of glaciers of the Subantarctic islands. *In* Kargel, J.S., Bishop, M.P., Kääb, A., Raup, B. & Leonard, G., *eds*, *Global land ice measurements from space: satellite multispectral imaging of glaciers*. Berlin: Springer, 759–780.

Cuffey, K.M. & Paterson, W.S.B. 2010. *The physics of glaciers*. Cambridge, MA: Academic Press, 704 pp.

Durand de Corbiac, H. 1970. La carte de reconnaissance des îles Kerguelen. *Comité National Français des Recherches Antarctiques*, **26**, 1–73.

Dyurgerov, M., Meier, M.F. & Bahr, D.B. 2009. A new index of glacier area change: a tool for glacier monitoring. *Journal of Glaciology*, **55**, 10.3189/002214309789471030.

Favier, V., Verfaillie, D., Berthier, E., Menegoz, M., Jomelli, V., Kay, J., *et al*. 2016. Atmospheric drying as the main driver of dramatic glacier wastage in the southern Indian Ocean. *Scientific Reports*, **6**, 10.1038/srep32396.

Frenot, Y., Gloaguen, J.C., Cannavacciuolo, M. & Bellido, A. 1998. Primary succession on glacier forelands in the sub-Antarctic Kerguelen Islands. *Journal of Vegetation Science*, **9**, 10.2307/3237225.

Frenot, Y., Gloaguen, J.C., van de Vijver, B. & Beyens, L. 1997. Datation de quelques sédiments tourbeux holocènes et oscillations glaciaires aux îles Kerguelen. *Comptes Rendus de l'Académie des Sciences*, **320**, 10.1016/S0764-4469(97)84712-9.

Frenot, Y., Gloaguen, J.C., Picot, G., Bougère, J. & Benjamin, D. 1993. *Azorella selago* Hook. used to estimate glacier fluctuations and climatic history in the Kerguelen Islands over the last two centuries. *Oecologia*, **95**, 140–144.

Gautier, I., Weis, D., Mennessier, J.-P., Vidal, P., Giret, A. & Loubet, M. 1990. Petrology and geochemistry of the Kerguelen Archipelago basalts (South Indian Ocean): evolution of the mantle sources from ridge to intraplate position. *Earth and Planetary Science Letters*, **100**, 59–76.

Giardino, C., Oggioni, A., Bresciani, M. & Yan, H. 2010. Remote sensing of suspended particulate matter in Himalayan lakes: a case study of alpine lakes in the Mount Everest region. *Mountain Research and Development*, **30**, 10.1659/MRD-JOURNAL-D-09-00042.1.

Gruber, S. 2012. Derivation and analysis of a high-resolution estimate of global permafrost zonation. *The Cryosphere*, **6**, 10.5194/tc-6-221-2012.

Hall, K. 1984. Evidence in favour of an extensive ice cover on sub-Antarctic Kerguelen Island during the Last Glacial. *Palaeogeography, Palaeoclimatology, Palaeoecology*, **47**, 225–232.

Hernández, A., Martin-Puertas, C., Moffa-Sánchez, P., Moreno-Chamarro, E., Ortega, P., Blockley, S., *et al*. 2020. Modes of climate variability: synthesis and review of proxy-based reconstructions through the Holocene. *Earth-Science Reviews*, **209**, 10.1016/j.earscirev.2020.103286.

Hugonnet, R., McNabb, R., Berthier, E., Menounos, B., Nuth, C., Girod, L., *et al*. 2021. Accelerated global glacier mass loss in the early twenty-first century. *Nature*, **592**, 10.1038/s41586-021-03436-z.

Ignéczi, A. & Nagy, B. 2013. Determining steady-state accumulation-area ratios of outlet glaciers for application of outlets in climate reconstructions. *Quaternary International*, **293**, 10.1016/j.quaint.2012.09.017.

Jomelli, V., Mokadem, F., Schimmelpfennig, I., Chapron, E., Rinterknecht, V., Favier, V., *et al*. 2017. Sub-Antarctic glacier extensions in the Kerguelen region (49°S, Indian Ocean) over the past 24,000 years constrained by ^{36}Cl moraine dating. *Quaternary Science Reviews*, **162**, 10.1016/j.quascirev.2017.03.010.

Jomelli, V., Schimmelpfennig, I., Favier, V., Mokadem, F., Landais, A., Rinterknecht, V., *et al*. 2018. Glacier extent in sub-Antarctic Kerguelen

https://doi.org/10.1017/S0954102023000378 Published online by Cambridge University Press

archipelago from MIS 3 period: evidence from ^{36}Cl dating. *Quaternary Science Reviews*, **183**, 10.1016/j.quascirev.2018.01.008.

Keeler, D.G., Rupper, S. & Schaefer, J.M. 2021. A first-order flexible ELA model based on geomorphic constraints. *MethodsX*, **8**, 10.1016/j.mex.2020.101173.

King, O., Dehecq, A., Quincey, D. & Carrivick, J. 2018. Contrasting geometric and dynamic evolution of lake and land-terminating glaciers in the central Himalaya. *Global and Planetary Change*, **167**, 46–60.

Li, C., Sonke, J.E., Le Roux, G., Van der Putten, N., Piotrowska, N., Jeandel, C., *et al*. 2020. Holocene dynamics of the southern westerly winds over the Indian Ocean inferred from a peat dust deposition record. *Quaternary Science Reviews*, **231**, 10.1016/j.quascirev. 2020.106169.

Linsbauer, A., Paul, F. & Haeberli, W. 2012. Modeling glacier thickness distribution and bed topography over entire mountain ranges with *GlabTop*: application of a fast and robust approach. *Journal of Geophysical Research - Earth Surface*, **117**, 10.1029/2011JF002313.

Magnin, F., Haeberli, W., Linsbauer, A., Deline, P. & Ravanel, L. 2020. Estimating glacier-bed overdeepenings as possible sites of future lakes in the de-glaciating Mont Blanc massif (western European Alps). *Geomorphology*, **350**, 10.1016/j.geomorph.2019.106913.

Mathieu, L., Byrne, P., Guillaume, D., van Wyk de Vries, B. & Moine, B. 2011. The field and remote sensing analysis of the Kerguelen Archipelago structure, Indian Ocean. *Journal of Volcanology and Geothermal Research*, **199**, 10.1016/j.jvolgeores.2010.11.013.

Matta, E., Giardino, C., Boggero, A. & Bresciani, M. 2017. Use of satellite and *in situ* reflectance data for lake water color characterization in the Everest Himalayan Region. *Mountain Research and Development*, **37**, 10.1659/MRDJOURNAL-D-15-00052.1.

Millan, R., Mouginot, J., Rabatel, A. & Morlighem, M. 2022. Ice velocity and thickness of the world's glaciers. *Nature Geosciences*, **15**, 10.1038/s41561-021-00885-z.

Nougier, J. 1970. Contribution à l'étude géologique et géomorphologique des îles Kerguelen. *Comité National Français des Recherches Antarctiques*, **27**, 440 pp. + 256 pp. + geologic map at 1:200 000.

Oppedal, L.T., Bakke, J., Paasche, Ø., Werner, J.P. & van der Bilt, W.G.M. 2018. Cirque Glacier on South Georgia shows centennial variability over the last 7000 years. *Frontiers in Earth Science*, **6**, 2.

Orsi, A.H., Whitworth III, T. & Nowlin, W.D. 1995. On the meridional extent and fronts of the Antarctic Circumpolar Current. *Deep-Sea Research I: Oceanographic Research Papers*, **42**, 10.1016/0967-0637 (95)00021-W.

Park, Y.-H., Vivier, F., Roquet, F. & Kestenare, E. 2009. Direct observations of the ACC transport across the Kerguelen Plateau. *Geophysical Research Letters*, **36**, 10.1029/2009GL039617.

Park, Y.-H., Park, T., Kim, T.-W., Lee, S.-H., Hong, C.-S., Lee, J.-H., *et al*. 2019. Observations of the Antarctic Circumpolar Current over the Udintsev Fracture Zone, the narrowest choke point in the Southern Ocean. *Journal of Geophysical Research - Oceans*, **124**, 10.1029/2019JC015024.

Paul, F. & Linsbauer, A. 2012. Modeling of glacier bed topography from glacier out-lines, central branch lines, and a DEM. *International Journal of Geographical Information Science*, **26**, 10.1080/ 13658816.2011.627859.

Peel, M.C., Finlayson, B.L. & McMahon, T.A. 2007. Updated world map of the Köppen-Geiger climate classification, *H*ydrology *and* Earth System *Sciences*, **11**, 10.5194/hess-11-1633-2007.

Pellitero, R., Rea, B., Spagnolo, M., Bakke, J., Hughes, P., Ivy-Ochs, S., *et al*. 2015. A GIS tool for automatic calculation of glacier equilibrium-line altitudes. *Computers & Geosciences*, **82**, 10.1016/ j.cageo.2015.05.005.

Pellitero, R., Rea, B.R., Spagnolo, M., Bakke, J., Ivy-Ochs, S., Frew, C.R., *et al*. 2016. *GlaRe*, a GIS tool to reconstruct the 3D surface of palaeoglaciers. *Computers & Geosciences*, **94**, 10.1016/j.cageo.2016.06.008.

Pohl, B., Saucède, T., Favier, V., Pergaud, J., Verfaillie, D., Féral, J.-P., *et al*. 2021. Recent climate variability around the Kerguelen Islands (Southern Ocean) seen through weather regimes. *Journal of Applied Meteorology and Climatology*, **60**, 10.1175/JAMC-D-20-0255.1.

Rabatel, A., Letréguilly, A., Dedieu, J.-P. & Eckert, N. 2013. Changes in glacier equilibrium-line altitude in the western Alps from 1984 to 2010: evaluation by remote sensing and modeling of the morpho-topographic and climate controls. *The Cryosphere*, **7**, 10.5194/ tc-7-1455-2013.

Renac, C., Kyser, K., Bowden, P., Moine, B. & Cottin, J.-Y. 2010. Hydrothermal fluid interaction in basaltic lava units, Kerguelen Archipelago (SW Indian Ocean). *European Journal of Mineralogy*, **22**, 10.1127/0935-1221/2009/0022-1993.

Ruiz, L., Bodin, X. 2015. Analysis and improvement of surface representativeness of high resolution Pléiades DEMs: examples from glaciers and rock glaciers in two areas of the Andes. *In* Jasiewicz, J., Zwoliński, Z., Mitasova, H. & Hengl, T., *eds*, *Proceedings of the Geomorphometry 2015 Conference*. Poznan: Adam Mickiewicz University in Poznań - Institute of Geoecology and Geoinformation, International Society for Geomorphometry, 223–226.

Schaefer, J.M., Codilean, A.T., Willenbring, J.K., Lu, Z.-T., Keisling, B., Fülöp, R.-H., *et al*. 2022. Cosmogenic nuclide techniques. *Nature Reviews Methods Primers*, **2**, 10.1038/s43586-022-00096-9.

Shugar, D.H., Burr, A., Haritashya, U.K., Kargel, J.S., Watso, C.S., Kennedy, M.C., *et al*. 2020. Rapid worldwide growth of glacial lakes since 1990. *Nature Climate Change*, **10**, 10.1038/s41558-020-0855-4.

Torsnes, I., Rye, N. & Nesje, A. 1993. Modern and Little Ice Age equilibrium-line altitudes on outlet valley glaciers from Jostedalsbreen, western Norway: an evaluation of different approaches to their calculation. *Arctic and Alpine Research*, **25**, 10.1080/00040851.1993.12002990.

Vallon, M. 1977a. Bilans de masse et fluctuations récentes du glacier Ampère (Iles Kerguelen, T.A.A.F.). *Zeitschrift für Gletscherkunde und Glazialgeologie*, **13**, 57–85.

Vallon, M. 1977b. Topographie sous-glaciaire du glacier Ampère (iles Kerguelen, TAAF). *Zeitschrift für Gletscherkunde und Glazialgeologie*, **13**, 37–55.

van der Bilt, W.G.M., Bakke, J., Werner, J.P., Paasche, Ø., Rosqvist, G. & Vatle, S.S. 2017. Late Holocene glacier reconstruction reveals retreat behind present limits and two-stage Little Ice Age on subantarctic South Georgia. *Journal of Quaternary Sciences*, **32**, 10.1002/jqs.2937.

Van der Putten, N., Stieperaere, H., Verbruggen, C. & Ochyra, R. 2004. Holocene palaeoecology and climate history of South Georgia (sub-Antarctica) based on a macrofossil record of bryophytes and seeds. *The Holocene*, **14**, 10.1191/0959683604hl714rp.

Van der Putten, N., Verbruggen, C., Björck, S., Michel, E., Disnar, J.-R., Chapron, E., *et al*. 2015. The Last Termination in the South Indian Ocean: a unique terrestrial record from Kerguelen Islands (49°S) situated within the Southern Hemisphere westerly belt. *Quaternary Science Reviews*, **122**, 142–157.

Verfaillie, D. 2014. *Suivi et modélisation du bilan de masse de la calotte Cook aux iles Kerguelen. Lien avec le changement climatique*. PhD thesis, Université de Grenoble, 275 pp.

Verfaillie, D., Charton, J., Schimmelpfennig, I., Stroebele, Z., Jomelli, V., Bétard, F., *et al*., 2021. Evolution of the Cook Ice Cap (Kerguelen Islands) between the last centuries and 2100 ce based on cosmogenic dating and glacio-climatic modelling. *Antarctic Science*, **33**, 10.1017/S0954102021000080.

Verfaillie, D., Favier, V., Dumont, M., Jomelli, V., Gilbert, A., Brunstein, D., *et al*. 2015. Recent glacier decline in the Kerguelen Islands (49°S, 69°E) derived from modeling, field observations, and satellite data. *Journal of Geophysical Research - Earth Surface*, **120**, 10.1002/2014JF003329.

Wang, X., Chai, K.G., Liu, S.Y., Wei, J., Jiang, Z. & Liu, Q. 2017. Changes of glaciers and glacial lakes implying corridor-barrier effects and climate change in the Hengduan Shan, southeastern Tibetan Plateau. *Journal of Glaciology*, **63**, 10.1017/jog.2017.14.